STUDIES OF AREA-SELECTIVE ATOMIC LAYER DEPOSITION USING COMPETITIVE ADSORPTION

A Thesis

Presented to the Faculty of the Graduate School

of Cornell University

In Partial Fulfillment of the Requirements for the Degree of

Master of Science

by

Heng-Ray Chuang

August 2023

ABSTRACT

Atomic layer deposition (ALD) is an important thin film deposition technique which enables scientists to deposit highly conformal films and control film thickness at angstrom level. Contrary to conventional semiconductor processing, ALD is a bottom-up process. Since multiple lithography and etching are not used, edge placement error is eliminated, and energy consumption can be reduced. Due to these great advantages, ALD can be potentially applied in next-generation device fabrication. In this research, a custom-built quartz crystal microbalance (QCM) was used to study ALD and area-selective ALD (AS-ALD).

A novel aluminum precursor and Tris(dimethylamino)cyclopentadienyl Zirconium (ZyALD) were investigated by using the QCM system. Temperature windows were studied, and pristine ALD recipes were developed. Additionally, both precursors were studied in AS-ALD via using competitive adsorption or small blocking molecules. Co-adsorbate was applied to compete with the novel aluminum precursor for available binding sites on the substrate surface. In AS-ALD for ZyALD, a silane blocking molecule was introduced to passivate the surface. The QCM results show that ALD growth rate can be attenuated by using both blocking mechanisms.

BIOGRAPHICAL SKETCH

Heng-Ray Chuang was born in Tainmu, Taiwan in 1997. After graduating from the Affiliated Senior High School of National Taiwan Normal University (HSNU), he attended National Cheng Kung University (NCKU) to study materials science. The classes he took at NCKU provided him an excellent grounding in materials science. In his third semester at NCKU, he decided to transfer to National Tsing Hua University (NTHU) to pursue his bachelor's degree. During his time at NTHU, he had learned various materials and he found that electronic materials were fascinating. He joined Engstrom Research Group at Cornell University in 2021 and started researching atomic layer deposition (ALD). During his time to date in the research group, he acquired knowledge in surface science and operated an ultra-high vacuum system. The experience and training he gained from Cornell will help his career in semiconductor industry.

ACKNOWLEDGMENTS

Firstly, I would like to thank my parents for their support. In addition to financial support, they also mentally supported me when I was frustrated. Additionally, I would like to thank the professors at NCHU and NTHU who wrote my recommendation letter for my grad school application. Without their help, I would never have the chance to study at Cornell. I would also like to thank everyone in Engstrom Research Group and DiStasio Research Group. We have done an excellent work during the past two years. Furthermore, I would like to express my gratitude to all my friends at Cornell CBE, including my friends in Tester Group, Hanrath Group, DeLisa Group, and Metaverse. Finally, I would like to thank Glenn at Cornell CBE who provided technical support for our research.

TABLE OF CONTENTS

LIST OF FIGURES

1 Introduction

1.1 Background

Moore's law is an observation proposed by Gordon Moore, which states that the number of transistors on integrated circuits doubles every two years [1]. Although Moore's law is not a physical law of nature, it approximately described the development of semiconductor industry in the past decades. Sizes of electronic devices have been continuously reduced to follow Moore's law. However, as the dimensions of devices continues to shrink, traditional semiconductor processing has reached bottlenecks. To continue Moore's law, developing new technologies for next-generation devices is urgent.

Top-down processing has been widely used in semiconductor fabrication, which includes repeated thin film deposition, photolithography, and etching [2]. To continue downscaling electronic devices, interest in creating nanoscale structures has increased. Nevertheless, challenges emerged when using top-down processing to fabricate nanoscale patterns. For instance, it is extremely difficult to perfectly align nanoscale features during photolithography and etching. Edge placement errors has become one of the challenges in semiconductor processing [3]. Additionally, repeated photolithography and etching steps consume huge amount of energy. Clearly, it is important to develop a new technique to overcome these challenges.

1.2 Atomic layer deposition

Atomic layer deposition (ALD) is a promising technique for nanomanufacturing. In contrast with traditional semiconductor fabrication, ALD is a bottom-up processing. Through utilizing ALD technique, semiconductor engineers can create nanoscale patterns on a wafter without using photolithography and etching. This great advantage enables semiconductors to be fabricated economically so that energy can be used efficiently. Moreover, ALD is a self-aligned process, which circumvents the misalignment caused by photolithography in traditional semiconductor processing [4]. Additionally, ALD possesses other advantages, including angstrom level control of film thickness and high conformality of deposited films [5]. Due to these outstanding features, ALD has become a vitally important technology for the next-generation semiconductor fabrication.

A single ALD cycle is composed of two half cycles, precursor and co-reactant exposure, separated by inert gas purge. It can be expressed in the following form:

Precursor | Purge | Co-reactant | Purge

Both precursor and co-reactant are carried by inert gas in gaseous phase, followed by an inert gas purge. The purpose of applying inert gas purge is to remove remnant chemicals in the reactor after each chemical dose. Typically, the inert gas used in ALD is nitrogen or argon. Contrary to chemical vapor deposition (CVD), each ALD cycle has only one kind of chemical in the reactor at once. In the first half cycle, precursor molecules occupy all the available binding sites on the substrate surface. The self-terminated surface prevents further precursor doses to react with the substrate. This is

known as self-limiting effect, which is the most important nature of ALD [6]. In the second half cycle, co-reactant molecules irreversibly chemisorb on the substrate via legend exchange. As precursor saturates on the surface, co-reactant binds to the surface until the surface is saturated with co-reactant. The surface is then transformed from precursor terminated to co-reactant terminated, which enables precursor dosed in the next ALD cycle reacts with the surface. The ALD cycle is applied repeatedly until the deposited film reaches a desired thickness.

Due to the feature of self-limiting, an ideal ALD growth rate is at a constant. Therefore, constant growth per cycle (GPC) has become an important indicator of ALD. However, Sønsteby *et al*. indicated that GPC in ALD might not be a constant and pointed out several misconceptions related to ALD [7]. GPC is strongly dependent on the reactive sites on the surface while the number of reactive sites can be varied during an ALD process. The morphology of the film could evolve over time, resulting in different numbers of available bonding site. As long as the surface is saturated, the process is still considered as ALD, even though GPC is inconsistent. In addition, Sønsteby et al. pointed out that a temperature window does not necessarily exist in ALD. Temperature window is a range of temperature in which GPC remains constant. The upper bound of the range is decomposition temperature of the precursor, while the lower bound of the range is the lowest temperature required for overcoming energy barrier in chemical reaction. Although temperature window is observed in many ALD experiments, it does not necessarily exist ALD. The number of reactive sites and film morphology could be strongly temperature dependent, resulting in inconsistent GPC. However, once self-limiting is observed, the process is still considered as ALD. To

sum up, constant GPC and temperature window are promising indicators of ALD, but surface saturation is the only determining characteristic of ALD.

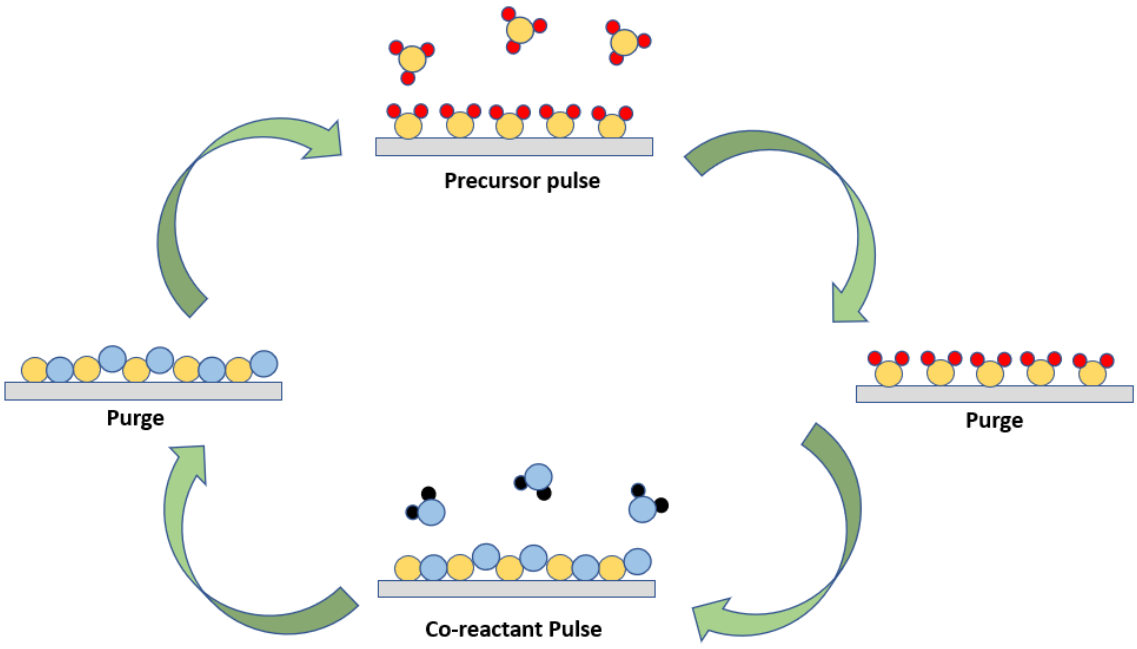

Figure 1 Schematic of an ALD cycle

1.3 Area-selective atomic layer deposition

Area-selective atomic layer deposition (AS-ALD) is a branch of ALD research which is becoming increasingly important as device features continue to decrease. In AS-ALD, the thin film is only deposited on one surface, and not another, dependent on the chemical composition of these surfaces. Through understanding different intrinsic properties between materials, such as chemical reactivity, area-selectivity can be achieved without any pretreatment on the surfaces [8]. However, as the interest in nanofabrication enhanced, the few AS-ALD processing cannot meet the increased market demand. Therefore, other pathways to increase selectivity are investigated, and combinations of different materials in AS-ALD are explored.

Definition of selectivity is widely accepted as the equation proposed by Gladfelter [9]:

$$S_{ASD} = \frac{D_{gs} - D_{ns}}{D_{gs} + D_{ns}}$$

In this equation, S_{ASD} represents the quantified selectivity in AS-ALD. D_{gs} and D_{ns} denote the thickness of film deposited on the growth surface (GS) and the non-growth surface (NGS), respectively. S_{ASD} equals to one when AS-ALD has perfect selectivity, while S_{ASD} equals to zero when the film is deposited without having any selectivity.

AS-ALD can be achieved with the help of the third species applied in ALD, including self-assembled monolayers (SAMs), small blocking molecules, and co-adsorbates. The third species is named differently because they achieve selectivity via different mechanisms.

Self-assembled monolayers (SAMs) are applied before ALD, which increase selectivity through forming passivation layer on the substrate surface [10]. Typically, SAMs consist of a functional headgroup, backbone made from alkyl chain, and an inert group at the end of the tail [11]. The functional headgroup selectively finds reactive sites on the non-growth surface (NGS), but not on the growth surface (GS). Hence, only the NGS is covered with SAMs and the growth is blocked there. The inert group passivates the surface while the alkyl chain prevents precursor from reaching the surface. SAMs with a longer backbone provide better selectivity because precursor is less likely to diffuse to the surface. Additionally, passivation layer formed by SAMs is highly ordered and dense because of van der Waals force between those long alkyl chains [12]. Despite these outstanding properties, there are several drawbacks of SAMs. Most of the SAMs have low vapor pressure because of its large molecular weight and therefore it cannot be transported in gaseous phase by conventional ALD system. Wet chemistry is applied to coat SAMs properly on the substrate surface [13]. Nevertheless, wet chemistry is time-consuming and sometimes it takes more than a day to complete the process [14]. The low throughput of wet chemistry is not desired for high volume manufacturing. Besides losing capability with ALD process, SAMs is also incompatible with plasma, which is widely used as co-reactant in ALD. Furthermore, in some cases SAMs block NGS and part of the adjacent GS because of its large volume [15]. Due to these drawbacks, interest has been increased to substitute other blocking molecules for SAMs.

Small blocking molecules consist of functional groups and inert groups. When small blocking molecules are applied, its functional headgroups selectively chemisorb

to the NGS, and inert groups passivate the surface [16]. The deficiency in alkyl backbone makes small blocking molecules have lower molecular weight and higher vapor pressure than SAMs. Hence, small blocking molecules can be applied to ALD systems and meet the requirements for high-volume nanomanufacturing [17]. Compared to SAMs, small blocking molecules are less likely to block GS adjacent to NGS because of its small volume. These outstanding properties attract people's interest in small blocking molecules. Yarbrough *et al*. studied AS-ALD using trimethylaluminum and triethylaluminum as the precursor, water as the co-reactant, and alkoxysilanes as the blocking molecules [18]. Copper and silica were soaked in gaseous alkoxysilane before the ALD cycle started. Their result shows alkoxysilanes inhibits the growth on silica in the first ten ALD cycles, and the selectivity increases as the number of methoxy groups on silane increases. Although passivation layer formed by small blocking molecules could be damaged during ALD, it can be repaired through reapplying blocking molecules [19]. Mameli *et al*. used acetylacetone as the blocking molecule, bis(diethylamino)silane as the precursor, and O_2 plasma as the co-reactant [20]. They reapplied blocking molecule in each ALD cycle. The three-step ALD cycle can be expressed as:

Blocking molecule | Purge | Precursor | Purge | Co-reactant | Purge

The result shows that growth was attenuated on SiO_2, GeO_2, and SiN_x. Due to deficiency in van der Waal force, it is difficult for small blocking molecules to form a closely packed passivation layer. To overcome this challenge, Xu *et al*. sequentially dosed two different sizes of blocking molecules, bis(dimethylamino)-dimethylsilane and (N,N-dimethylamino)-trimethylsilane [21]. Although growth was attenuated when

either molecule was dosed, nucleation delay could be further extended when both molecules were applied together. The result can be explained by deposition on reactive sites in the gap between blocking molecules. A smaller blocking molecule can fill into the gap and eliminate the potential pathways for growth.

Co-adsorbate is applied before, during, and after precursor pulse in AS-ALD to compete for binding sites with precursor on NGS [22]. The ALD cycle can be expressed in the following form:

Co-adsorbate | Precursor/Co-adsorbate | Co-adsorbate | purge | Co-reactant | purge

Ideally, co-adsorbate has no interactions with GS, but weakly bonds to NGS and blocks ALD growth on it. Moreover, an ideal co-adsorbate should not interact with precursor. In AS-ALD, co-adsorbate firstly saturates the NGS, occupying all the available bonding sites on it. During the co-exposure of precursor and co-adsorbate, co-adsorbate competes with precursor for binding sites on NGS. Due to the weak bonding between co-adsorbate and NGS, co-adsorbate can be removed during the purge of first half reaction, leaving NGS clean. This novel co-adsorbate blocking mechanism is firstly proposed by Dr. Engstrom at Cornell University and it has not been widely studied. Suh *et al.* investigated this blocking mechanism using 3-hexyne as co-adsorbate, tetrakis(ethylmethylamido)zirconium (TEMAZ) as precursor, and water or oxygen as co-reactants [23]. The result shows nucleation delay on copper surface and zirconia deposition on silica, which is supported by the density functional theory (DFT) calculation performed by Dr. DiStasio.

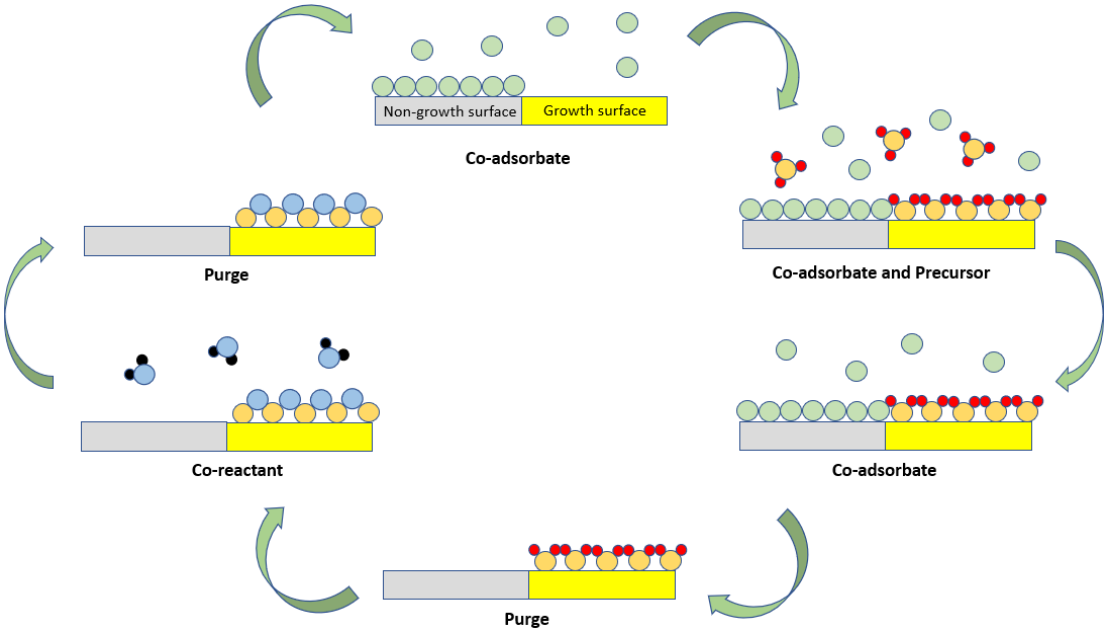

Figure 2 Schematic of an AS-ALD cycle (using co-adsorbate to block precursor)

2 Experimental Setup

2.1 Chamber Setup

A quartz crystal microbalance (QCM) was used to monitor thin film deposition in real time. The system design is illustrated in Figure 3 (made by Amy You). When experiments were conducted, pneumatic gate valve (P25) was opened so that the reactor was pumped by the process pump (Edwards E2M30). On the other hand, the manual gate valve (M8) was closed to isolate the reactor from turbomolecular pump (Pfeiffer Balzers TPU 060) and pump 2 (Edwards E2M28). The reactor pressure was controlled by a throttle valve (MKS 253B-1-40-1) and measured by baratron.

Cylinder one contains argon, which serves as backside purge and carrier gas for reactive species (i.e., precursors, co-reactants and co-adsorbates) delivered to the reactor for subsequent depositions. Backside purge is an inert gas flow beneath the crystal in QCM, which passes by manual valve (M6) and translator. The purpose of flowing backside purge is to prevent unwanted deposition under the crystal. Carrier gas either flows through or flows over bubblers and delivers chemicals to the reactor in gas phase. Cylinder two contains argon, which serves as dead zone flows or source of argon plasma in plasma ALD. Cylinder three contains oxygen, which serves as source of oxygen plasma in plasma ALD. Cylinder four contains a mixture of hydrogen (3%) and argon (97%), which serves as dead zone flows.

Oscillation frequencies of crystals purchased from Inficon Inc. were measured. The change in oscillation frequency can be converted to mass change via Sauerbrey equation:

$$\Delta m = -\frac{A\sqrt{\rho_q \mu_q}}{2f_0^2}\Delta f$$

Δm denotes mass change on the crystal. Δf and f_0 denotes the oscillation frequency change and the resonant frequency of the crystal. ρ_q, μ_q, and A represents density, shear modulus, and surface area of the crystal, respectively. To do data analysis of deposition, the Sauerbrey equation is utilized to convert from frequency values measured on the crystal to apparent mass density changes on the crystal surface.

2.2 Delivery System

The delivery system consists of four panels. Panel A contains mass flow controller (MFC) A, E, F and G, as shown in figure 3. MFC A controls QCM back side purge; MFC E controls the argon flow through the plasma generator; MFC F controls the oxygen flow through the plasma generator; MFC G controls dead zone flows. Panel B, C and D are connected to the feedthrough and deliver reactive species from bubblers to the reactor. On the downstream of panel B and C, there are three-way valves which control the carrier gas either flow to the feedthrough or to pump 2. The delivery line on the downstream of panel B, C and D are wrapped with heating tapes to prevent chemical condensation on the inner wall.

2.3 Load crystal and wafers

Crystal and wafers were loaded from the load lock. Since the system was operated under high vacuum, it must be vented before opening the load lock door. After crystal and sample holder were moved back from the furnace to the load lock, manual valve (M8) was closed to isolate load lock from turbomolecular pump, manual gate valve (M7) was closed to isolate the load lock from reactor, manual valve (M6) was closed and manual valve (M5) was opened, and argon was flowed from cylinder one. Load lock pressure reached atmospheric pressure after eighteen minutes due to the sagging of the bellows if argon flow was set at 200sccm. Crystal was placed into the crystal holder and secured by the latch on QCM. Wafers were placed onto sample holder by a metal tweezer. Crystal snatcher, crystal holder, plastic and metal tweezers were wiped with isopropyl alcohol before being used. After crystal and wafers were loaded, load lock door was closed. Manual valve (M8) was opened to pump down the load lock, and manual gate valve (M7) was opened. Crystal and sample holder were moved back to reactor afterwards.

2.4 Sample preparation

AC-cut crystals purchased from Inficon Inc. were used, which were composed of metal electrode on the bottom and metal coating on the surface. Metal coating was either gold, copper, or cobalt. These crystals have nominal frequency at 6 MHz, and are optimized at 120˚C or 285˚C. Bare silicon wafers and copper-coated silicon wafers

were cut into 1.15 in by 0.35 in. All the wafers were cleaned by UV-ozone cleaner before being used. To remove oxide on the surface, copper-coated silicon wafers were annealed at 180˚C in the reactor with argon flowing over the surface.

2.5 Materials

Three precursors were studied: trimethylaluminum, nitrogen containing aluminum precursor (NcAP, from our industry collaborator), and Tris(dimethylamino)cyclopentadienyl Zirconium. Water with ultra-high purity was used as co-reactant. In the study of area-selective ALD, isopropyl alcohol (anhydrous, 99.5%, Sigma-Aldrich) and silane blocking molecule were used as co-adsorbate and blocking molecule, respectively. All these chemicals were stored in stainless steel bubblers and placed in the ampoules under panel B, C and D. To ensure reactive species were filled into the bubbler without any contamination from ambient molecules, such as water, they were loaded either in the glovebox at Cornell Center for Materials Research (CCMR) or in the glove bag. Argon with ultra-high purity was used as carrier gas, and argon-hydrogen mixture (3% hydrogen) was used as dead zone flows.

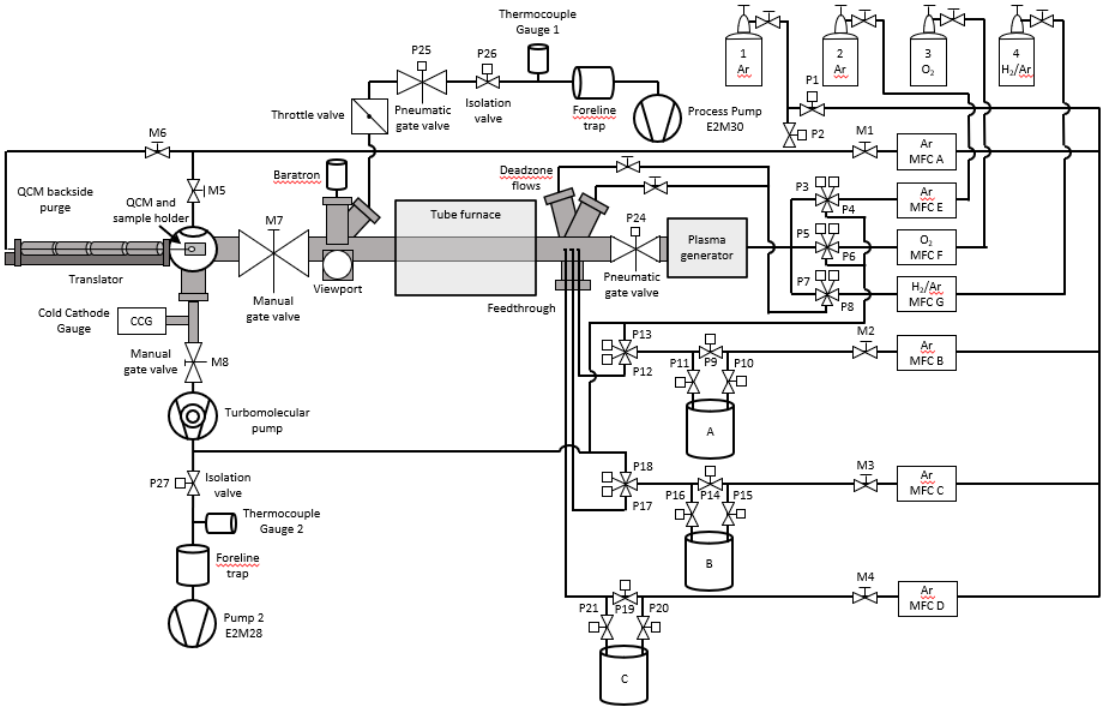

Figure 3 Schematic of custom-built quartz crystal microbalance

3. System Modifications

3.1 TMA|water ALD before system modifications

It is important to demonstrate the basic ability of the QCM system to conduct ALD before studying ALD in depth. Hence, a well-investigated ALD process of using trimethylaluminum as precursor and water as co-reactant was conducted. In the first half reaction, one or two of the methyl groups on trimethylaluminum react with the hydrogen on the hydroxyl group and form methane. The surface is transformed from hydroxyl group to O-Al$(CH_3)_x$, where x equals to one or two. In the second half reaction, one of the hydrogens on water reacts with methyl groups on the surface and form methane. After the second half reaction, the surface is saturated by hydroxyl groups again.

In our experiments, trimethylaluminum and water were stored in a stainless-steel bubbler and placed in an ice bath because of the high vapor pressure of both chemicals. Furnace temperature was set at 120˚C, and chamber pressure was maintained at 1.5 torr during depositions. To prevent chemical condensation on the inner wall of delivery line, delivery lines of trimethylaluminum and water were heated to 80˚C and 100˚C, respectively. Carrier gas was set to 10sccm of argon flow through the trimethylaluminum and the water bubbler. QCM back side purge was set to 50sccm of argon to prevent deposition under the crystal. Each of the dead zones was purged with 10sccm of the gas from cylinder four, which was composed of 97% of argon and 3% of hydrogen. Each ALD cycle is composed of 1 second dose of trimethylaluminum,

followed by 29 second of purge, followed by 2 second dose of water, followed by 28 second of purge. A gold-coated crystal which is optimized at 120˚C was loaded. Before staring the experiment, the crystal surface was saturated with hydroxyl group.

When carrier gas flows through a bubbler, both the upstream and downstream pneumatic valves are opened so that carrier gas can enter the bubbler and deliver chemical to the reactor, as Figure 4a shows. On the other hand, carrier gas flows over a bubbler when the upstream pneumatic valve is closed while the downstream pneumatic valve is opened, as Figure 4b shows.

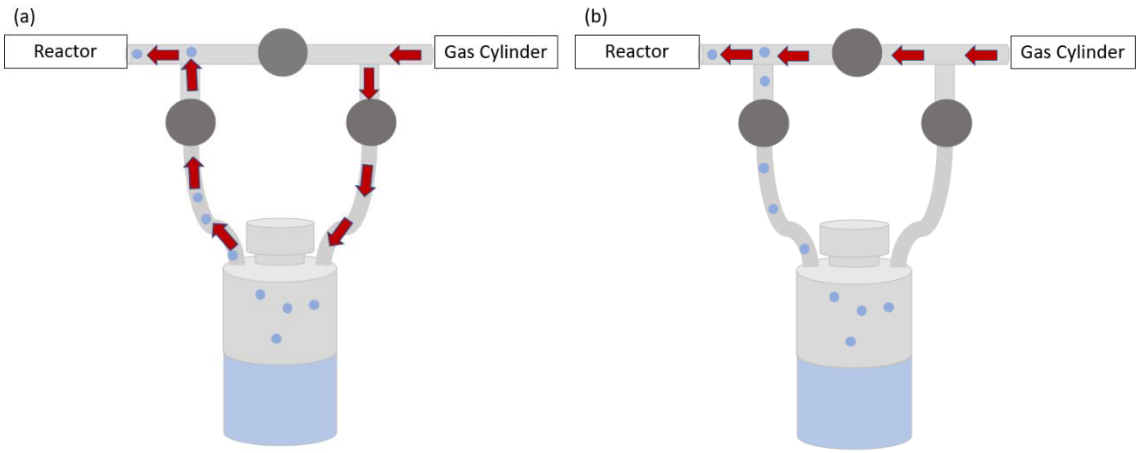

Figure 4 (a) Schematic of carrier gas flowing through bubbler (b) Schematic of carrier gas flowing over bubbler.

There are 20 deposition cycles in each experiment, as Figure 5 shows. Growth per cycle (GPC) was inconsistent, which accelerated in the beginning and decelerated at the end of the deposition process. By zooming in on cycle one and nine, as shown in Figure 6a and b, a different trend of the surface density change was observed. During the trimethylaluminum pulse, the surface density increased by 40 $ng.cm^{-2}$ in cycle one and 60 $ng.cm^{-2}$ in cycle nine. In the step of water pulse, the surface density decreased in cycle one but increased in cycle nine. Additionally, surface density did not increase immediately when trimethylaluminum was applied. The inconsistent GPC, trend of surface density change, and nucleation delay were not expected to be observed.

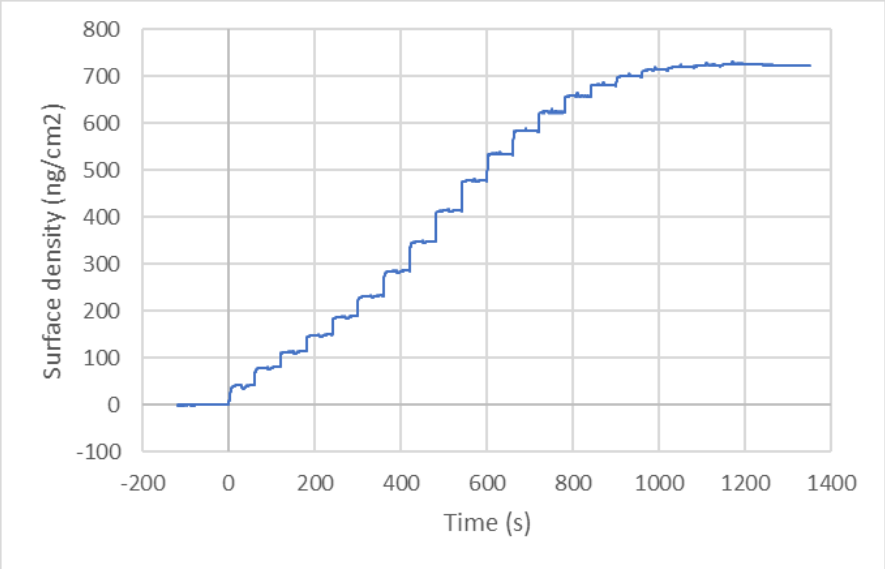

Figure 5 QCM result from 20 cycles of deposition using trimethylaluminum as precursor and water as co-reactant. (2/11/2022, Run 2)

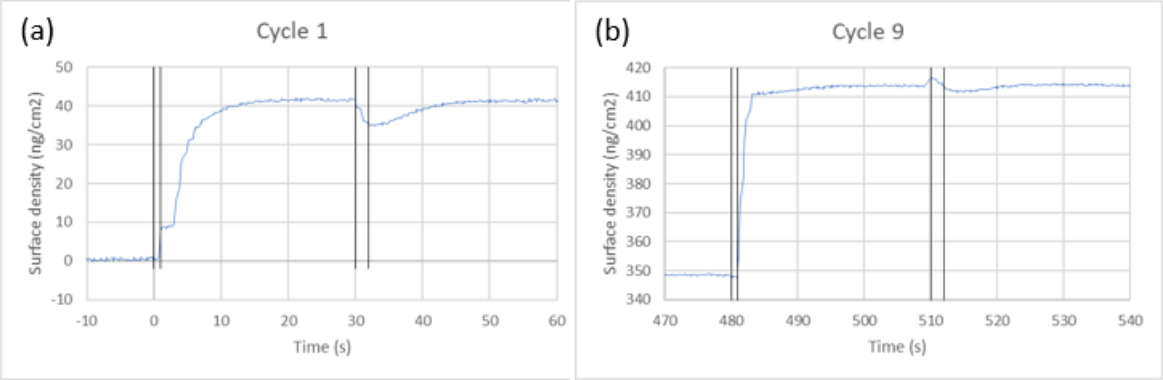

Figure 6 QCM results of single ALD cycles, (a) cycle one, (b) cycle nine.

The ALD process was repeated on a trimethylaluminum-saturated surface. Each ALD cycle consists of 1 second dose of trimethylaluminum, followed by 29 second of purge, followed by 2 second dose of water, followed by 58 second of purge. The furnace temperature, chamber pressure, QCM back side purge, dead zone purge, and carrier gas were maintained at the same conditions.

As Figure 7 shows, nucleation delay was observed because there were no hydroxyl groups on the surface in the beginning of the deposition process. Since density of alumina is $3.97 g.cm^{-3}$, alumina film with thickness of 1Å has surface density of $39.7 ng.cm^{-2}$. At the end of the experiment, GPC reached approximately $400 ng.cm^{-2}.cycle^{-1}$ ($10.07 Å.cycle^{-1}$), as shown in Figure 8. However, it is widely

accepted that GPC in this process is roughly 1Å. For instance, Salami *et al*. reported 1.1Å of GPC in the same process [24].

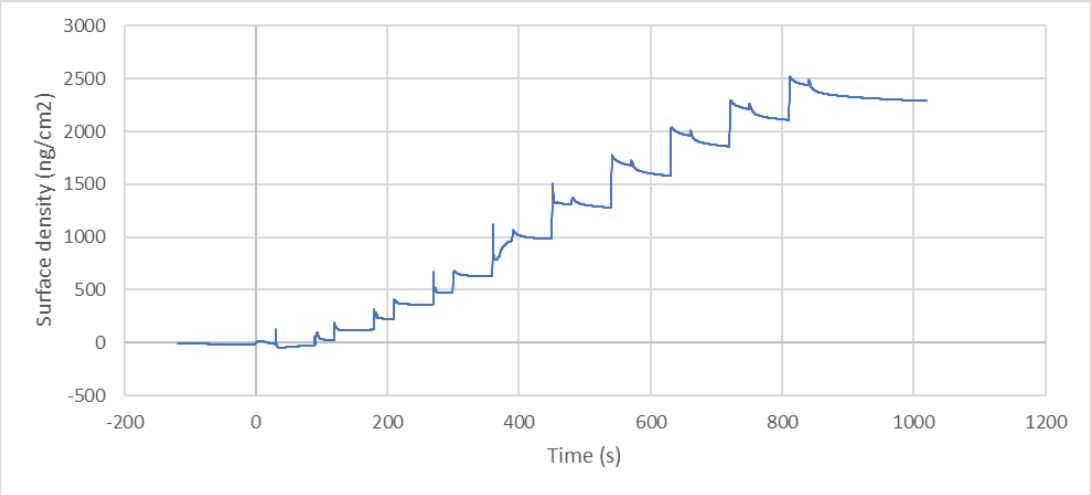

Figure 7 QCM result from 10 cycles of deposition using trimethylaluminum as precursor and water as co-reactant. (3/2/2022, Run 14)

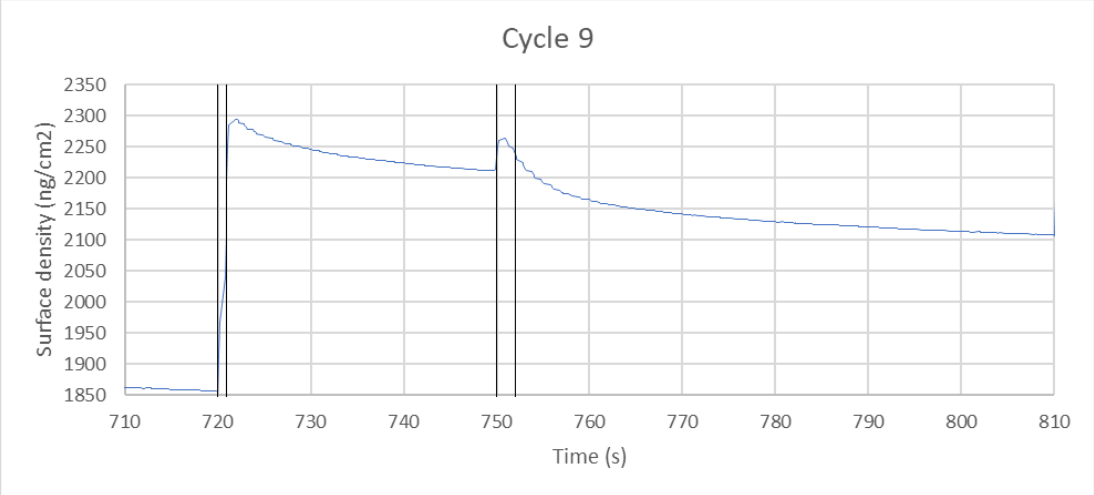

Figure 8 Cycle nine of the QCM result.

Due to the observation of these atypical data, including inconsistent growth rate, unexpected nucleation delay, and extremely high GPC, it was concluded that the experiments done in the system was chemical vapor deposition (CVD) instead of ALD. Hence, several modifications were made to eliminate the sources of errors in the system.

3.2 Modifications of the QCM reactor

Sønsteby et al. reported that cold spots and dead zones in deposition tools could be possible sources of errors [4]. Water, a common oxygen source in ALD, could condense on cold spots and slowly release during ALD. Dead zones can be sources of molecules lingering in the reactor, resulting in unwanted precursor and co-reactant pulses overlap. These two sources of errors make the whole process become chemical vapor deposition (CVD) instead of ALD.

There were three dead zones in the system, as circled in red in Figure 9. To eliminate these dead zones, argon from cylinder two is flowed through the plasma generator, and gas from cylinder four is flowed through the other two dead zones, as shown in Figure 10. Additionally, a thick deposited layer on the inner wall of the reactor was accumulated from previous experiments. This porous layer can store water from water pulses and release it during purge or precursor pulses, making the whole process become CVD. Hence, the reactor was removed from the system and cleaned. The reactor was wiped with isopropyl alcohol to remove powder on the surface. Afterwards, both sides of the reactor were submerged in Alconox solution and

sonicated for more than eight hours. The flanges used to connect reactor and system were cleaned by standard vacuum cleaning process. Firstly, flanges were submerged in trichloroethylene and sonicated for thirty minutes to remove hydrocarbons. Next, these flanges were rinsed with DI water to remove trichloroethylene on the surface. Afterwards, these flanges were sonicated by acetone and isopropyl alcohol sequentially to remove hydroxyl groups and chlorine, respectively. After the standard vacuum cleaning, the reactor and flanges were assembled back to the system and baked for two days.

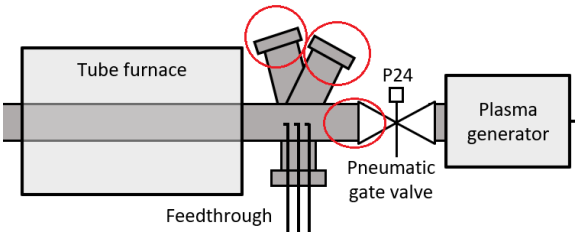

Figure 9 Schematic of the three dead zones before system modification.

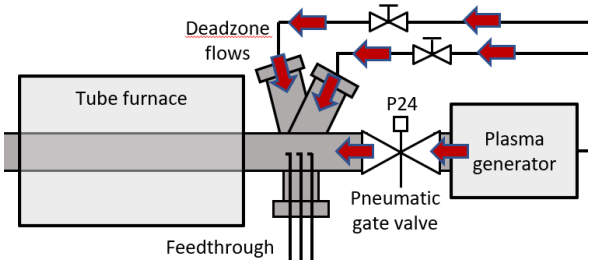

Figure 10 Schematic of the system modifications made for dead zone purges.

In addition to eliminating sources of water, two other modifications were made—feedthrough was modified, and the delivery line was shortened. Feedthrough in the initial design directed flows to one of the dead zones, as Figure 11 shows, which could have increased lingering molecules in the reactor. Hence, the feedthrough was modified to deliver flows parallel to the reactor, as Figure 12 shows. Another problem in the system was the extremely long delivery line of precursor. Some unstable precursors could have decomposed before it reached the reactor. To solve the problem, the delivery line was shortened, and the whole was moved closer to the reactor. The heating tape on the delivery line was reinstalled in appropriate places to eliminate cold spots.

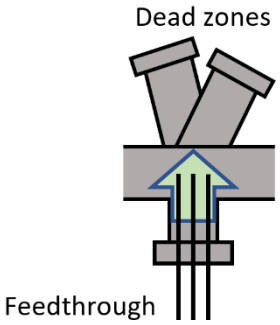

Figure 11 Schematic of feedthrough flows before modification.

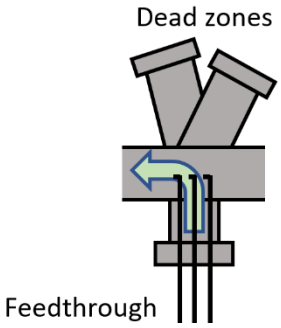

Figure 12 Schematic of feedthrough flows after modification.

3.3 TMA|water ALD after system modifications

After several modifications were made, an ALD process with 2 second dose of trimethylaluminum, followed by 28 second of purge, followed by 0.5 second dose of water, followed by 59.5 second of purge was done on a gold-coated crystal. The furnace temperature was set at 120˚C, and the chamber pressure was maintained at 1 torr. Trimethylaluminum and water bubbler were placed in an ice bath. Delivery lines of trimethylaluminum and water were heated to 110˚C and 80˚C, respectively. Carrier gas was set to 10sccm flow through the trimethylaluminum bubbler and 10sccm flow over the water bubbler. QCM back side purge was set to 50sccm of argon to prevent deposition under the crystal, and each of the dead zones was purged with 10sccm of the gas from cylinder four.

As Figure 13 shows, nucleation delay was observed on the gold surface because gold is not reactive to trimethylaluminum and water. As the experiment proceeded, the surface was gradually covered with alumina, which had a lower energy barrier for trimethylaluminum and water to bind to the surface. GPC accelerated and plateaued at around $1\text{Å}.\,\text{cycle}^{-1}$, as shown in Figure 14a and b. The consistent GPC implies that the surface was self-limiting, which is the most important feature of ALD. In addition, the growth rate is close to the value reported by other groups. Clearly, the system demonstrated the basic ability to conduct ALD.

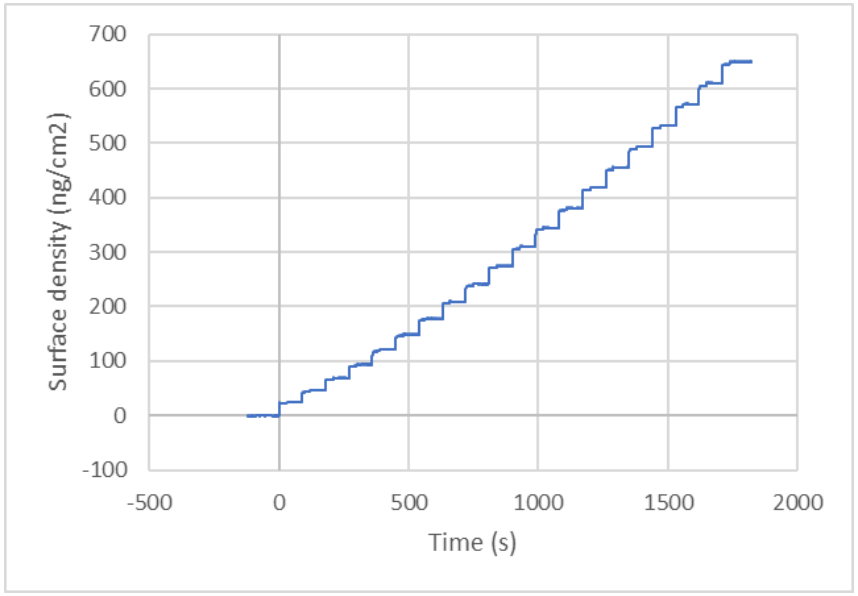

Figure 13 QCM result of TMA|water ALD after system modification. (2/4/2023, Run 1)

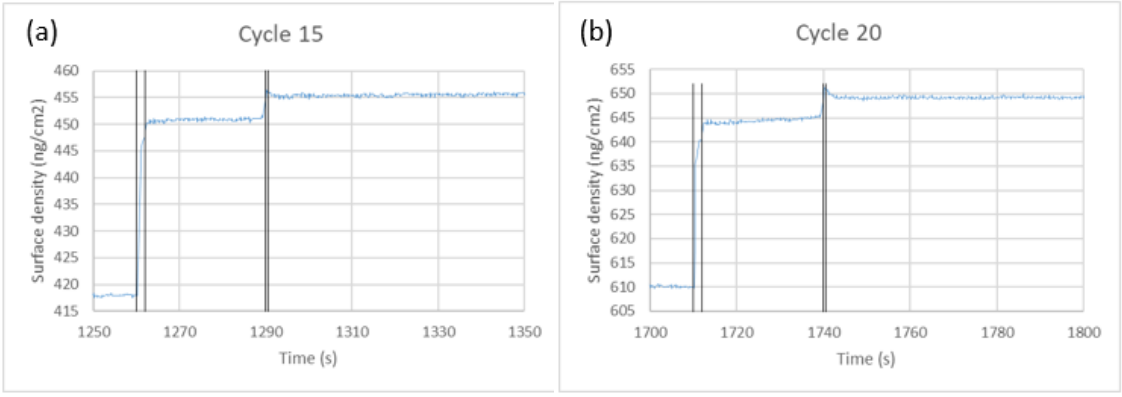

Figure 14 QCM results of single ALD cycles after system modification, (a) cycle fifteen, (b) cycle twenty.

4. Pristine NcAP|water ALD Study

4.1 NcAP pressure study

Trimethylaluminum is widely used in industry for alumina deposition while its high reactivity decreases selectivity in AS-ALD. For instance, Merkx *et al*. studied AS-ALD by depositing three aluminum containing precursors on an acetylacetone (Hacac) passivated surface [25]. The result shows that dimethylaluminum isopropoxide (DMAI) and tris(dimethylamino)aluminum (TDMAA) have a lower growth rate on the non-growth surface, compared to trimethylaluminum (TMA). Hence, nitrogen containing aluminum precursor (NcAP) was synthesized to potentially replace trimethylaluminum in alumina deposition.

To ensure NcAP can be delivered in gas phase, partial pressure of NcAP was measured in a pressure test. In an ALD process, chamber pressure was fixed by adjusting the throttle valve position. When chemical was dosed, throttle valve opened more to lower the abrupt pressure raise and maintain chamber pressure at the setpoint. In a pressure test, however, the throttle valve was fixed at a specific position. The chamber pressure was increased when the tested chemical was applied.

During the NcAP pressure test, the chamber temperature was maintained at 120˚C, and the throttle valve opening was fixed at 31.1%. Hence, the chamber pressure was maintained at 0.499 Torr before NcAP was introduced. The NcAP bubbler was placed in a heat bath and heated to 60˚C. The NcAP delivery line was heated to 80˚C to prevent precursor condensation on the inner wall. Carrier gas was set at 50sccm flow

through the NcAP bubbler. As Figure 15 shows, 200 seconds after the pressure was recorded, five NcAP pulses (flow through) was conducted. Each NcAP pulse includes 15 second dose of NcAP and 45 second of purge. When NcAP was introduced, the chamber pressure increased from 0.499 Torr to 0.509 Torr, indicating that vapor pressure of NcAP is 10 mTorr when NcAP is at 60˚C and carried by 50sccm of argon. The result shows that NcAP has a sufficiently high vapor pressure so that it can be delivered in gas phase and applied in ALD processes.

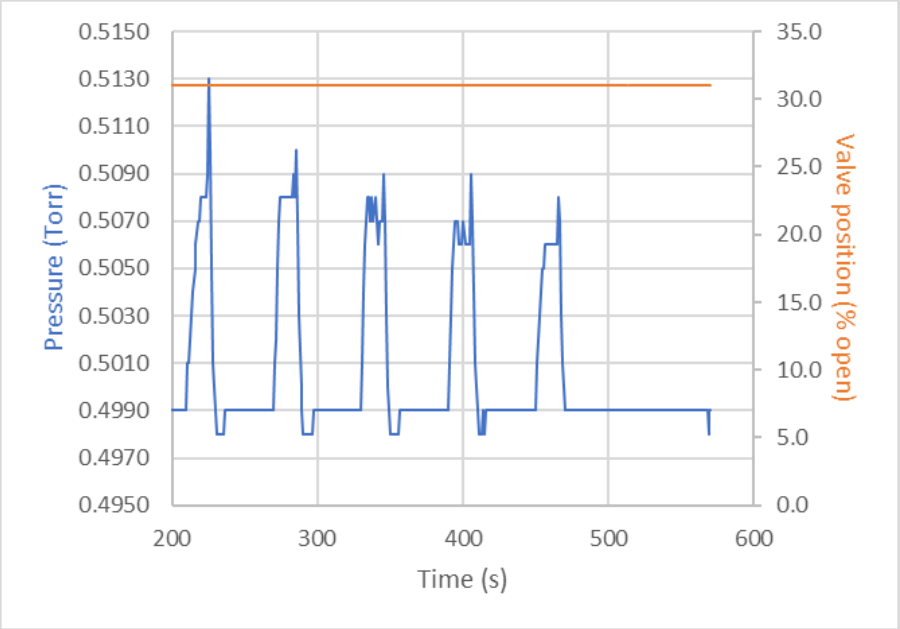

Figure 15 Pressure change during NcAP pressure test. (2/10/2022, Run 4)

4.2 Development of NcAP|water ALD recipe

Developing the baseline experiment of NcAP is vitally important since NcAP is a novel precursor and has not been published yet. In the pristine ALD process, the chamber pressure was set to 1 Torr. NcAP bubbler was placed in a heat bath and heated to 60˚C. Water bubbler was placed in an ice bath due to its high vapor pressure. Delivery lines of NcAP and water were heated to 100˚C and 60˚C, respectively. The pristine ALD can be expressed in the format:

NcAP | Purge | H_2O | Purge

A gold-coated crystal which is optimized at 120˚C was loaded and saturated with hydroxyl group on the surface before the experiment started. QCM back side purge was set to 50sccm of argon, and each of the dead zones was purged with 10sccm of gas from cylinder four (97% of argon and 3% of hydrogen). Carrier gas was set to 30sccm of argon flow through the NcAP bubbler and 10sccm of argon flow over the water bubbler.

The pristine ALD process was repeated at two different temperatures, 120˚C and 180˚C. At 120˚C, each ALD cycle included 360 second dose of NcAP, followed by 120 second of purge, followed by 1 second dose of water, followed by 119 second of purge. At 180˚C, the purge time in the second half cycle was extended to 179 seconds and other conditions were remained the same.

Figure 16 shows the surface density changed during the deposition process at 120˚C. The growth rate was nearly constant, showing a linear increase in the surface density. After ten cycles of ALD, the surface density increased by 376.5 $ng.cm^{-2}$,

which indicated that growth per cycle (GPC) was 37.65 ng.cm^{-2}.cycle^{-1} (0.95 Å.cycle^{-1}). Figure 17a to c are the surface density changes during cycle one, five and nine. By zooming in on single cycles, a long nucleation delay of NcAP on the crystal surface was observed, and surface density started increasing approximately after 200 seconds in the first half reaction. The surface density increased and plateaued, indicating that the surface was self-limited by NcAP. In the second half reaction, the surface density decreased when water was dosed, showing that ligand changed happened between water and NcAP and a heavy ligand was replaced by hydroxyl group.

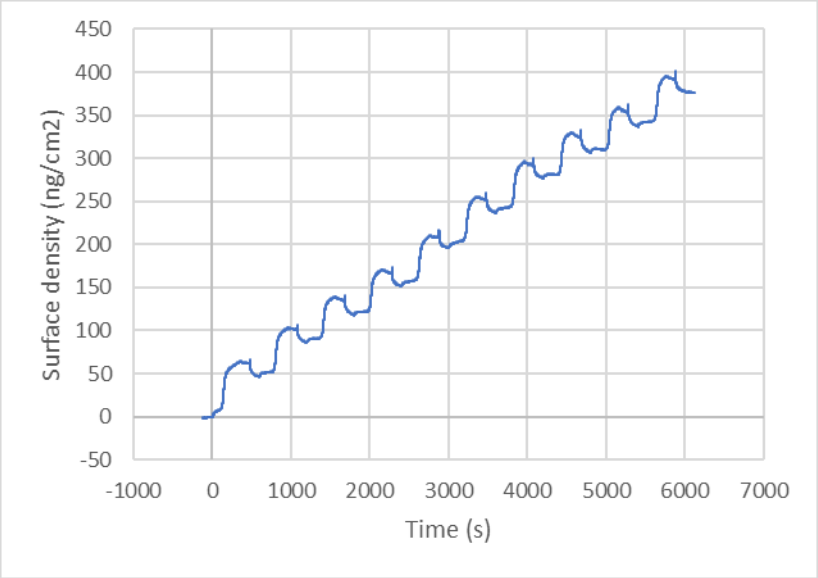

Figure 16 QCM result of NcAP|water at 120˚C. (5/31/2022, Run 5)

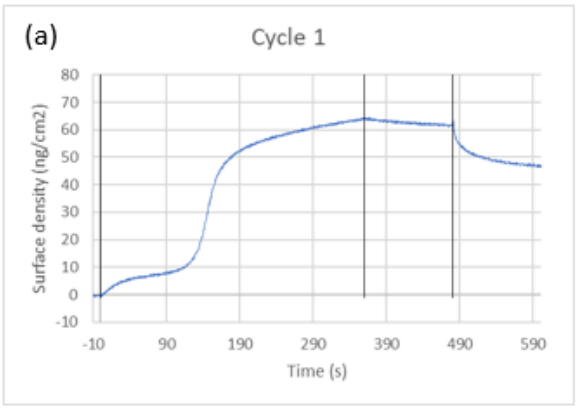

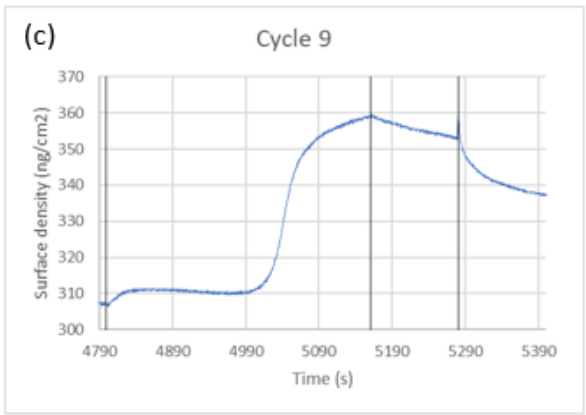

Figure 17 Single ALD cycles of NcAP|water at 120˚C, (a) cycle one, (b) cycle five, (c) cycle nine.

Figure 18 shows the result of the deposition process done at 180˚C. After ten cycles of deposition, the surface density increased by 348.4 $ng.cm^{-2}$, indicating that GPC was 34.84 $ng.cm^{-2}.cycle^{-1}$ (0.88 $Å.cycle^{-1}$). Although the value of GPC is close to the result obtained at 120˚C, the growth rate at 180˚C does not show a linearity. This is because the crystal used in this experiment is optimized at 120˚C, while the experiment was conducted at 180˚C. This kind of surface density fluctuation is called "drift", which means the change of surface density is caused by crystal itself rather than a real mass change on the surface. Figure 19a to c are the result of cycle one, five and nine in the deposition process. A long nucleation delay was observed, and the surface density also started increasing roughly after 200 seconds in the first half reaction. In the second half reaction, decrease in surface density was observed when water was introduced, showing the ligand exchange between NcAP and water.

To sum up, the process shows several features of ALD, including self-limiting on the surface and similar GPCs at 120˚C and 180˚C. At both temperatures, nucleation delay on the surface and ligand exchange between water and NcAP were observed.

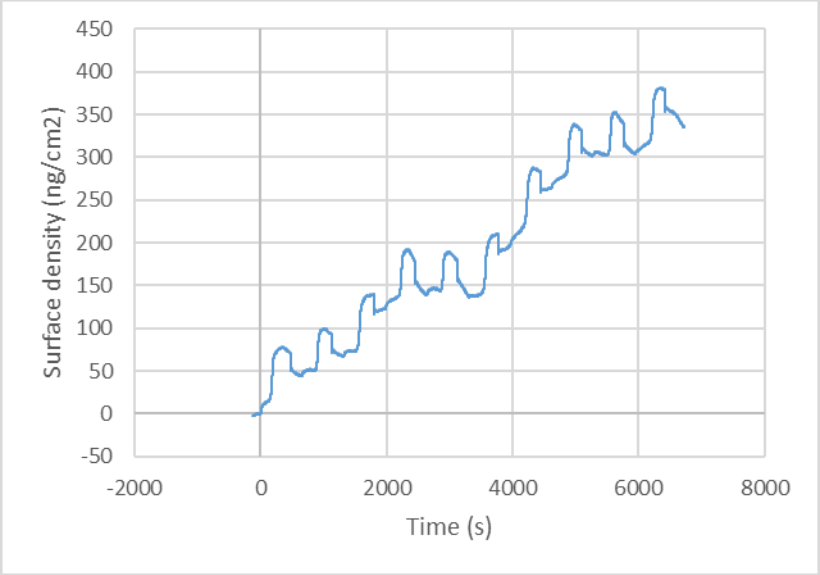

Figure 18 QCM result of NcAP|water at 180˚C. (6/1/2022, Run 8)

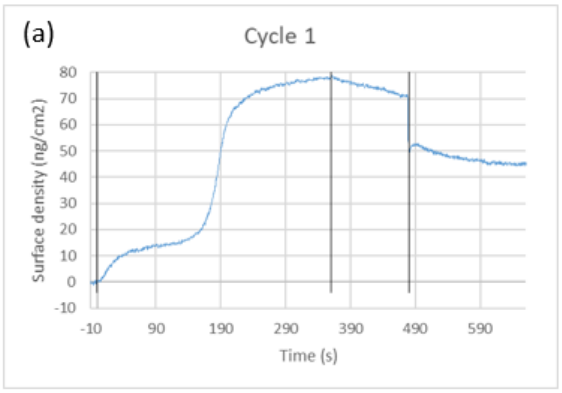

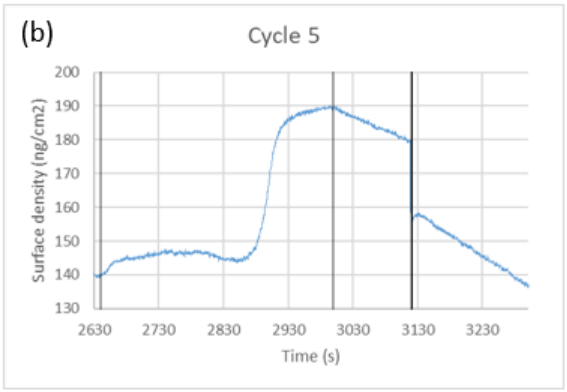

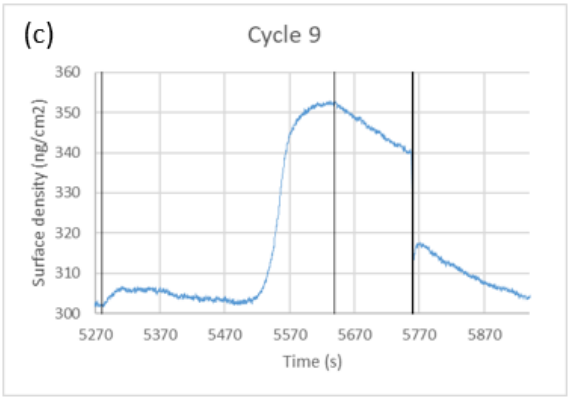

Figure 19 Single ALD cycles of NcAP|water at 180˚C, (a) cycle one, (b) cycle five, (c) cycle nine.

Although the deposition process mentioned above seems to be ALD, the six minutes dose of NcAP is unusually long, compared to other ALD processes. For instance, Soethoudt *et al*. deposited Ru, TiN, TiO_2 and HfO_2, using five seconds pulse of EBECHRu, 0.8 seconds pulse of $TiCl_4$, four seconds pulse of $Ti(OCH_3)_4$, and one second pulse of $HfCl_4$, respectively [26]. The long delivery line of NcAP could have resulted in molecular decomposition of NcAP before it was delivered to the reactor. Therefore, the delivery line was shortened and the whole panel was moved closer to the reactor, as mentioned previously in section 3.2.

The ALD process of NcAP was repeated at 120˚C after the delivery line was shortened. Each ALD cycle consists of 45 second dose of NcAP, followed by 60 second of purge, followed by 1 second dose of water, followed by 29 second of purge. A gold-coated crystal which is optimized at 120˚C was loaded and saturated with hydroxyl group on the surface before the experiment started. NcAP bubbler was placed in a heat bath and heated to 90˚C. Water bubbler was placed in an ice bath to lower water's vapor pressure. During the ALD process, chamber pressure was set to 1Torr. The delivery line of NcAP and water were heated to 110˚C and 80˚C, respectively. QCM back side purge was set to 50sccm of argon, and each of the dead zones was purge with 10sccm of gas from cylinder four (97% of argon and 3% of hydrogen). Carrier gas was set to 50sccm of argon flowing through the NcAP bubbler, and 10sccm of argon flowing over the water bubbler.

Figure 20 shows the real time surface density change during ten cycles of deposition. GPC was roughly at a constant, which was 76 $ng.cm^{-2}.cycle^{-1}$ (1.9 $Å.cycle^{-1}$). However, by zooming in on cycle one, five and nine, it is obvious that surface

density changed differently in both half reactions. As shown from Figure 21a to c, a 30 second nucleation delay was observed in cycle five and nine but not in cycle one. Additionally, in cycle five and nine, surface density decreased in the purge of first half reaction, which is unusual in an ALD process. When water was introduced, surface density decreased in cycle one, indicating that ligand exchange happened on the substrate surface. In cycle five and nine, however, there was nearly nothing changed when water was introduced. These inconsistencies between single cycles show that the deposition process is not exactly an ALD.

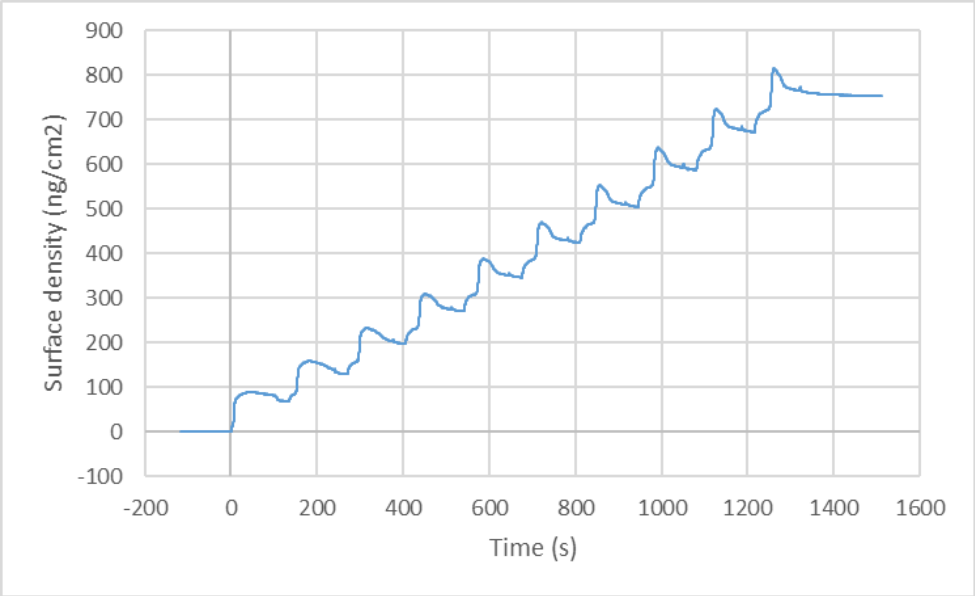

Figure 20 QCM result of NcAP|water ALD at 120˚C (after shortening NcAP delivery line). (6/17/2022, Run 7)

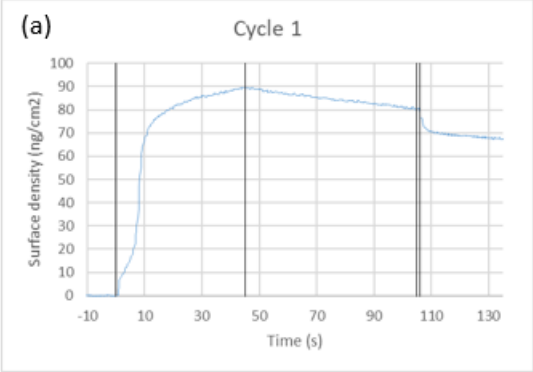

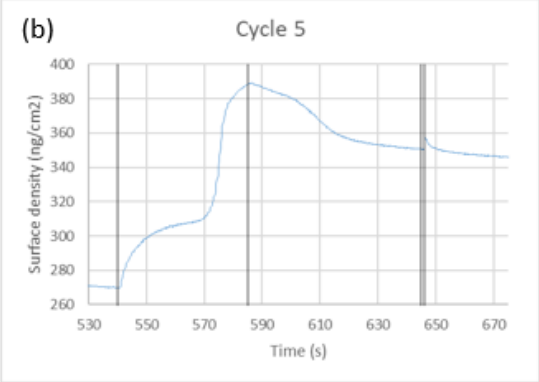

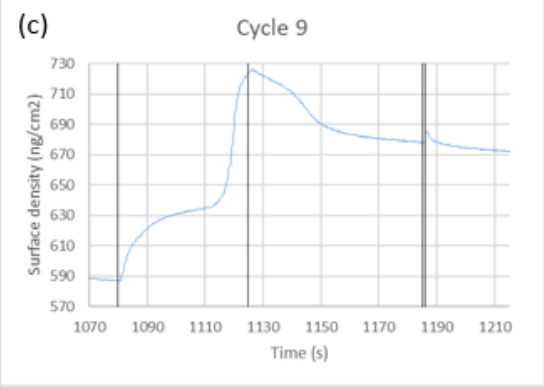

Figure 21 Single ALD cycles of NcAP|water at 120˚C (after shortening NcAP delivery line), (a) cycle one, (b) cycle five, (c) cycle nine.

4.3 NcAP|water ALD at 150˚C

The atypical shape of the QCM result is caused by insufficient long purge time so that NcAP and water pulses were overlapped. Hence, the deposition process with using NcAP as precursor and water as co-reactant was done again at 150˚C. Each ALD cycle is composed of 15 second dose of NcAP, followed by 45 second of purge, followed by 0.5 second dose of water, followed by 359.5 second of purge. A gold-coated crystal which is optimized at 120˚C was loaded and saturated with hydroxyl group on the surface before starting the deposition. NcAP bubbler was placed in heat bath and heated to 90˚C. Water bubbler was place in an ice bath to lower water's vapor pressure. During the ALD process, chamber pressure was maintained at 1 Torr. The delivery line of NcAP and water were heated to 110˚C and 80˚C, respectively. QCM back side purge was set to 50sccm of argon, and each of the dead zones was purged with 10sccm of gas from cylinder four (97% of argon and 3% of hydrogen). Carrier gas was set to 50sccm of argon flow through the NcAP bubbler and 10sccm of argon flow over the water bubbler.

Figure 22 shows the result obtained from QCM after ten cycles of deposition. The surface density linearly increased by 357.16 $ng.cm^{-2}$, indicating that GPC was nearly at 0.89 $Å.cycle^{-1}$. By zooming in on cycle one, five and nine, it is apparent that all the single cycles showed a similar trend of surface density change, as shown from Figure 23a to c. In the first half reaction, surface density increased by 90 $ng.cm^{-2}$ in the step of NcAP pulse and plateaued in the following purge. In the second half reaction, surface density significantly decreased by 25 $ng.cm^{-2}$ in the step of water pulse and

plateaued in the following purge. The result of ligand exchange between NcAP and water was consistent with the calculation made by Dr. DiStasio (Cornell Chemistry). The decrease of surface density in the purge was caused by crystal itself rather than a real mass change. Since the crystal was optimized at 120˚C while the deposition process was conducted at 150˚C, the QCM result could be dictated by drift.

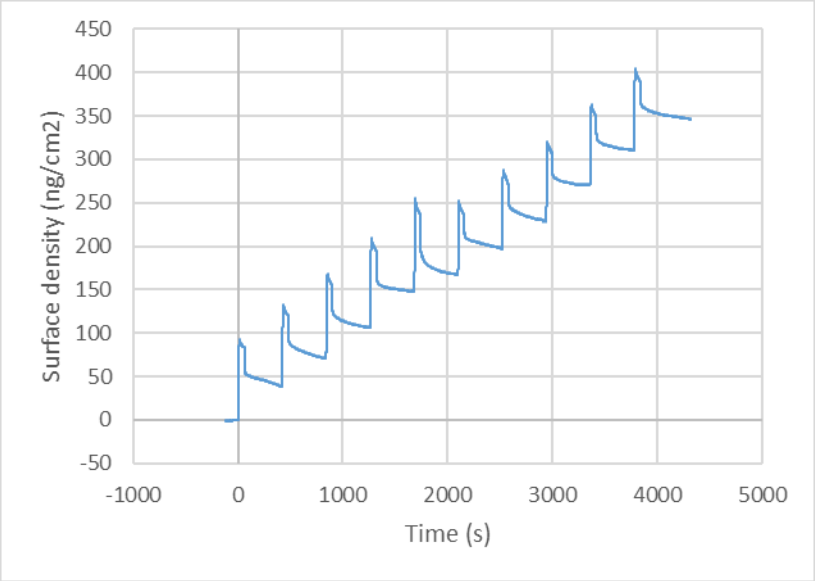

Figure 22 QCM result of NcAP|water at 150˚C (15 second dose of NcAP). (6/24/2022, Run 2)

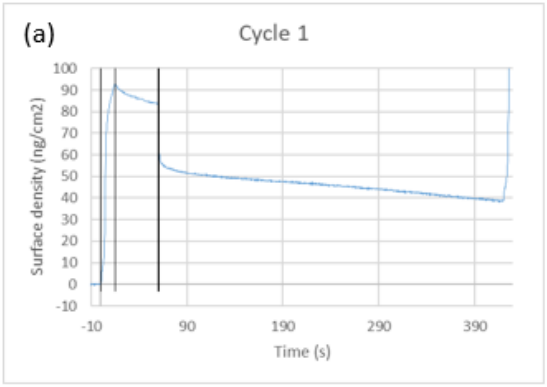

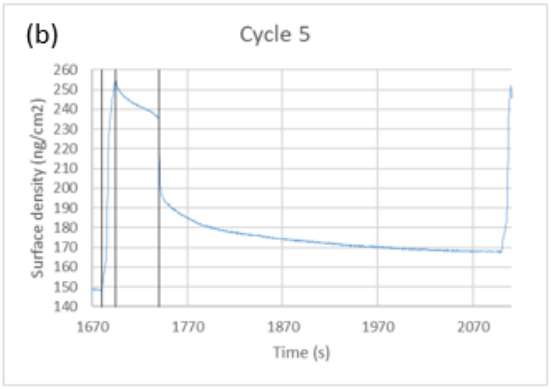

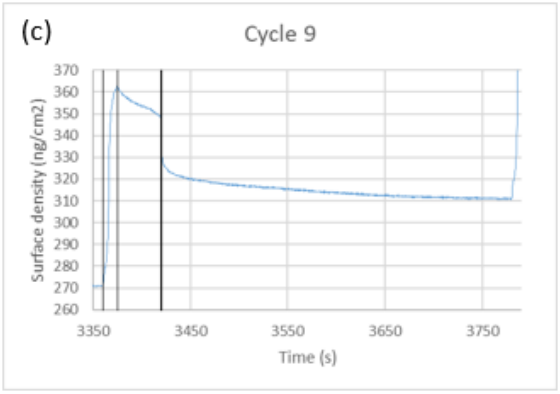

Figure 23 Single ALD cycles of NcAP|water at 150˚C (15 second dose of NcAP), (a) cycle one, (b) cycle five, (c) cycle nine.

To ensure the surface was fully saturated with precursor and co-reactant, the experiment was repeated at 150°C with an extension of NcAP dose. Each ALD cycle consists of 20 second dose of NcAP, followed by 40 second of purge, followed by 0.5 second of water, followed by 359.5 second of purge. A gold-coated crystal was loaded without any pretreatment. Other conditions were remained the same.

As Figure 24 shows, GPC was less than the result obtained from the previous NcAP deposition process. This is because the gold-coated crystal was not saturated with hydroxyl group on the surface when it was loaded. By zooming in on single cycles, nucleation delay was observed on the gold surface in the first several cycles, as shown in Figure 25a. However, it is obvious that change of surface density after cycle five showed an identical trend with the 15 second NcAP deposition process, as shown in Figure 25b and c.

These two experiments demonstrated that the recipe of depositing NcAP with using water as co-reactant at 150°C is well-developed. Moreover, the deposition process was proved to be an ALD process because saturation was observed on the surface and GPC did not increase as the increasing dose time of NcAP.

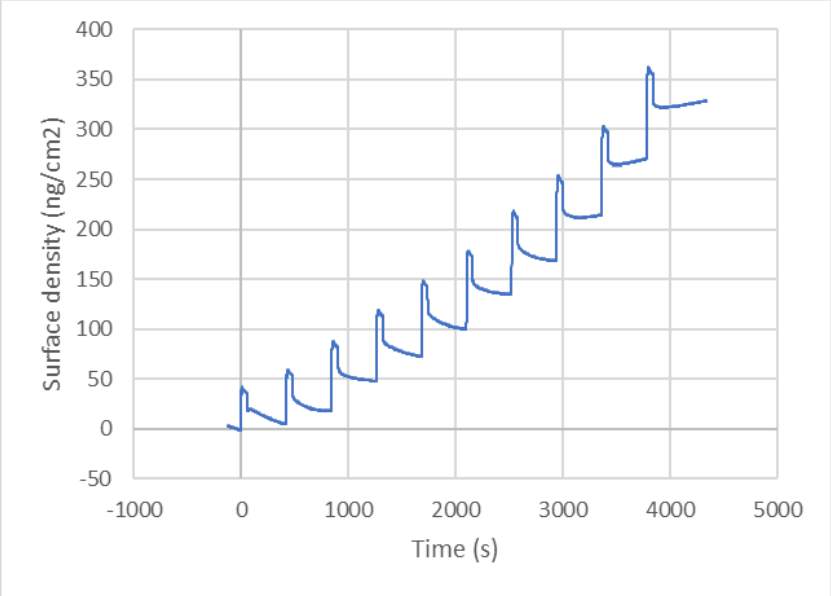

Figure 24 QCM result of NcAP|water at 150˚C (20 second dose of NcAP). (6/24/2022, Run 1)

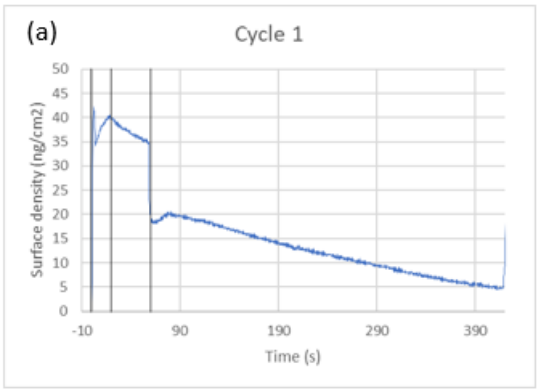

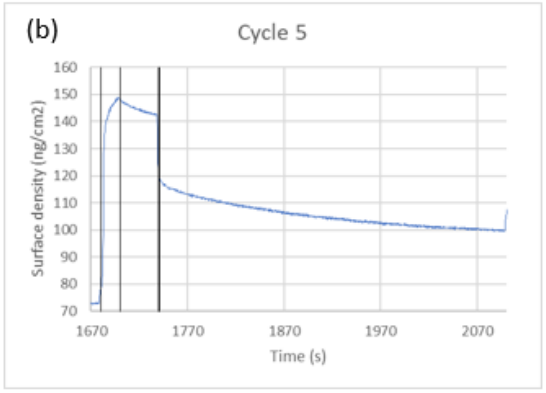

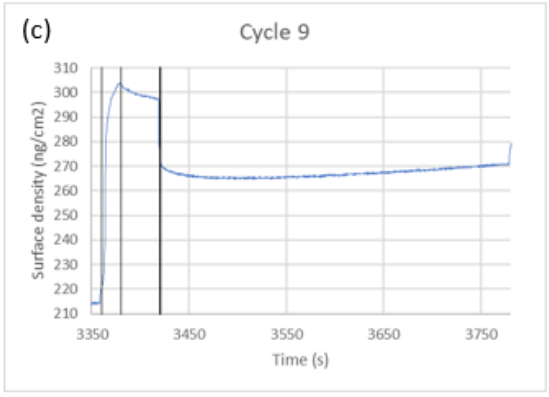

Figure 25 Single ALD cycles of NcAP|water at 150˚C (20 second dose of NcAP), (a) cycle one, (b) cycle five, (c) cycle nine.

4.4 NcAP|water ALD at 180˚C

The temperature widow was explored after determining the recipe of NcAP ALD process at 150˚C. Two ALD processes were done at 180˚C, one with 15 second dose of NcAP, followed by 45 second of purge, followed by 0.5 second dose of water, followed by 359.5 second of purge; the other one with 20 second dose of NcAP, followed by 40 second of purge, followed by 0.5 second dose of water, followed by 359.5 second of purge. A gold-coated crystal which is optimized at 120˚C was loaded and saturated with hydroxyl group on the surface before deposition started. The chamber pressure, carrier gas, QCM back side purge, bubbler temperatures, dead zone purge, and temperatures of delivery lines were at the same condition used at 150˚C.

Figure 26 shows the QCM result for the deposition process which contains 15 second dose of NcAP. The linear growth shows that GPC is nearly a constant. After ten cycles of deposition, the surface density increased by 400 $ng.cm^{-2}$, showing that GPC was nearly 1 $Å.cycle^{-1}$. By zooming in on cycle one, five and nine, a similar trend of surface density change was observed, as shown from Figure 27a to c. The surface density increased by 85 $ng.cm^{-2}$ during NcAP pulses, then slightly decreased in the following purge. In the step of water pulse, the surface density decreased by 20 $ng.cm^{-2}$ due to ligand exchange. The surface density changes in single cycles are very consistent, showing that the process could be an ALD process.

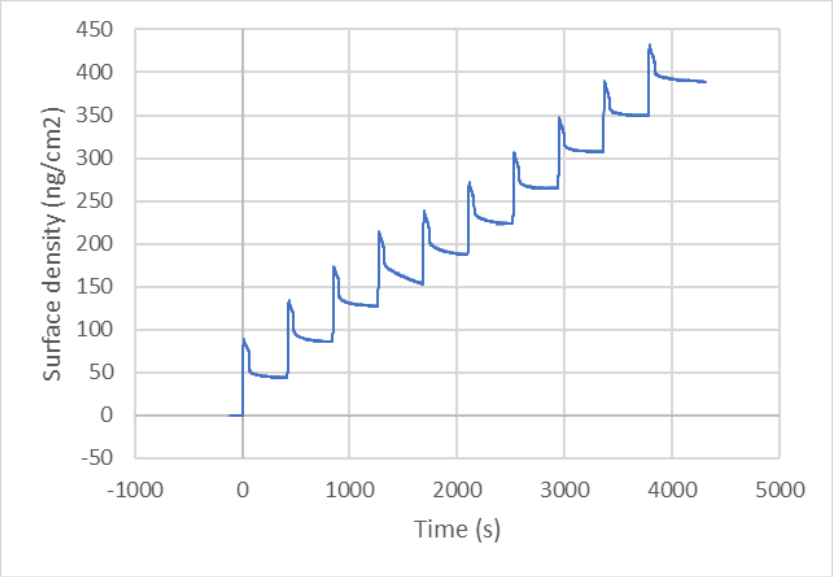

Figure 26 QCM result of NcAP|water at 180˚C (15 second dose of NcAP). (6/25/2022, Run 3)

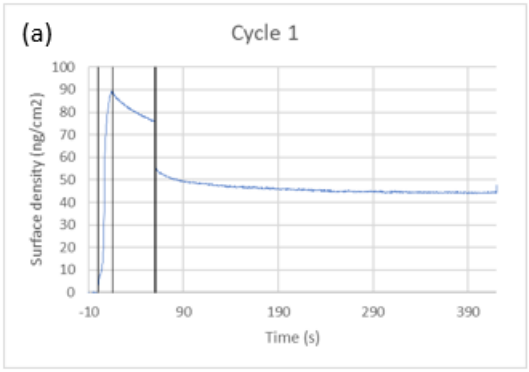

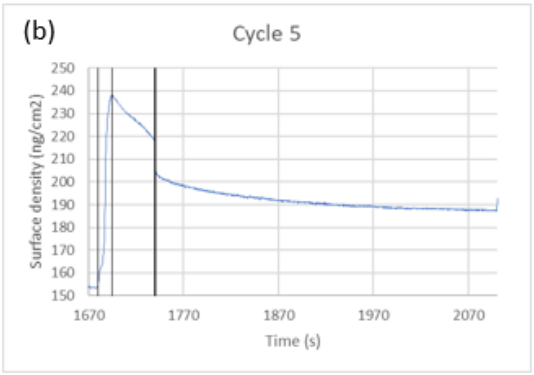

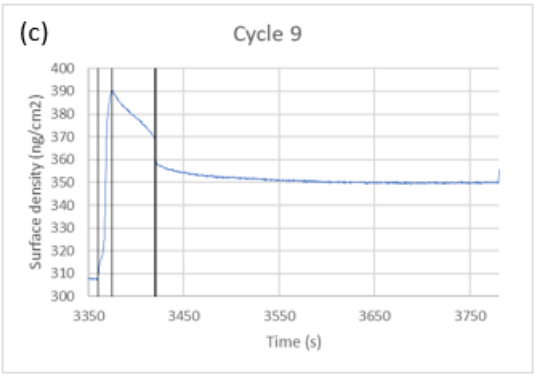

Figure 27 Single ALD cycles of NcAP|water at 180˚C (15 second dose of NcAP), (a) cycle one, (b) cycle five, (c) cycle nine.

To ensure the surface was fully saturated with NcAP, the dose time of NcAP was extended to 20 seconds. Figure 28 shows the QCM result after ten cycles of deposition. The surface density still linearly increased by 400 $ng.cm^{-2}$, showing that deposition rate was around 1 $Å.cycle^{-1}$. By zooming in on cycle one, five and nine, it was observed that the surface density changed similarly in each deposition cycle, as shown from Figure 29a to c. The surface density increased by 85 $ng.cm^{-2}$ during NcAP pulses and decreased by 20 $ng.cm^{-2}$ during water pulses. Additionally, surface density slightly decreased in the purge after NcAP pulses but remained at a constant in the purge after water pulses.

Deposition rate did not increase with increasing dose time of NcAP, indicating that self-limiting occurred on the surface. Additionally, surface density changed consistently in single cycles. Therefore, the deposition process was proved to be an ALD process.

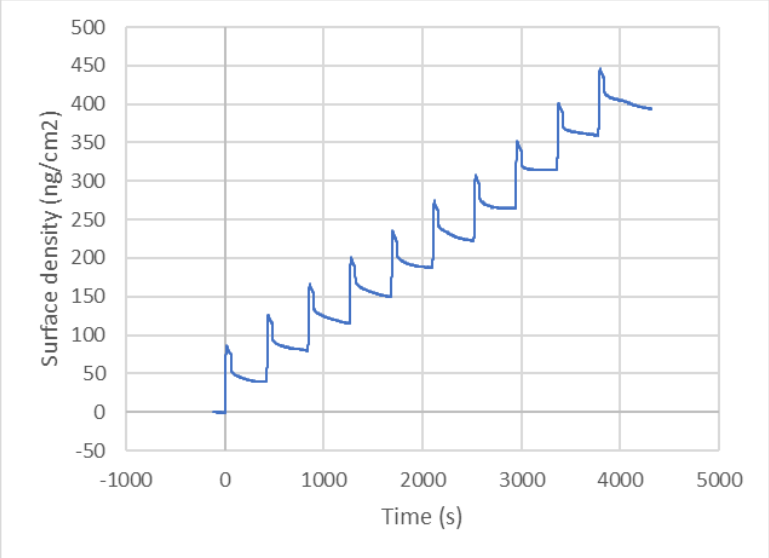

Figure 28 QCM result of NcAP|water at 180˚C (20 second dose of NcAP). (6/25/2022, Run 4)

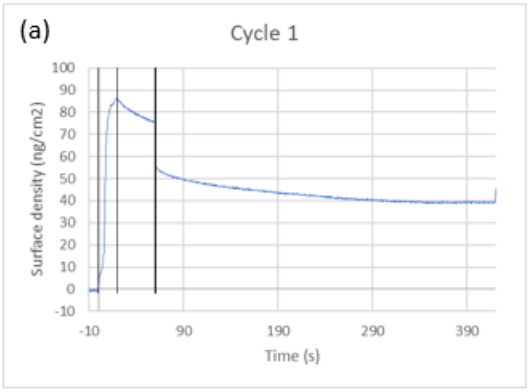

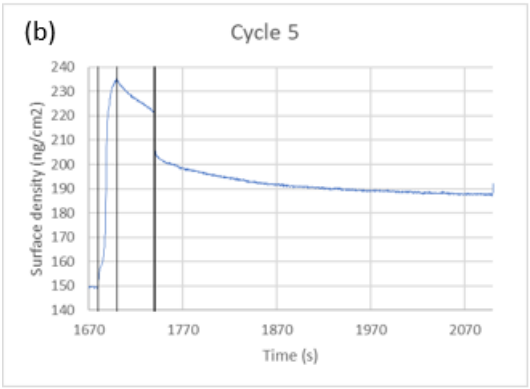

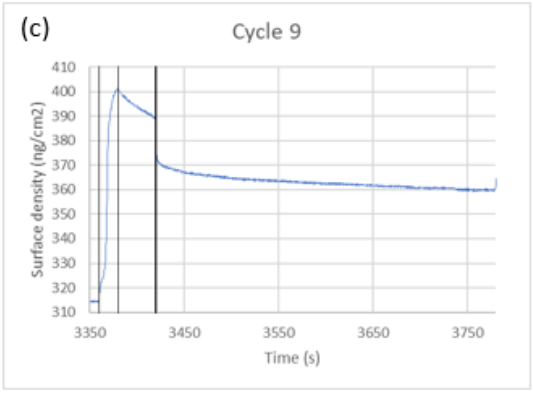

Figure 29 Single ALD cycles of NcAP|water at 180˚C (20 second dose of NcAP), (a) cycle one, (b) cycle five, (c) cycle nine.

4.5 NcAP|water ALD at 255˚C

Two deposition processes were done at 255˚C, one with 15 second dose of NcAP, followed by 45 second of purge, followed by 0.5 second dose of water, followed by 359.5 second of purge; the other one with 20 second dose of NcAP, followed by 40 second of purge, followed by 0.5 second dose of water, followed by 359.5 second of purge. A gold-coated crystal which is optimized at 285˚C was loaded and saturated with hydroxyl group on the surface before each deposition process started. The chamber pressure, carrier gas, QCM back side purge, bubbler temperatures, dead zone purge and temperatures of delivery lines were at the same condition used at 150˚C.

Figure 30 shows the QCM result obtained from the deposition process which contains 15 second dose of NcAP. The surface density increased by 308 $ng.cm^{-2}$ after ten cycles of deposition. However, it was not increased linearly because of the drift from the extremely long purge in the second half reaction, as shown in Figure 31 (cycle 7). By zooming in on cycle one, five, and nine, it was obvious that the change of surface density was similar in the first three steps of the deposition process, as shown from Figure 32a to c. The surface density roughly increased by 65 $ng.cm^{-2}$ in the step of NcAP pulse and decreased by 20 $ng.cm^{-2}$ when water was introduced. The consistency was evidence of ALD, although the QCM result was dictated by the drift.

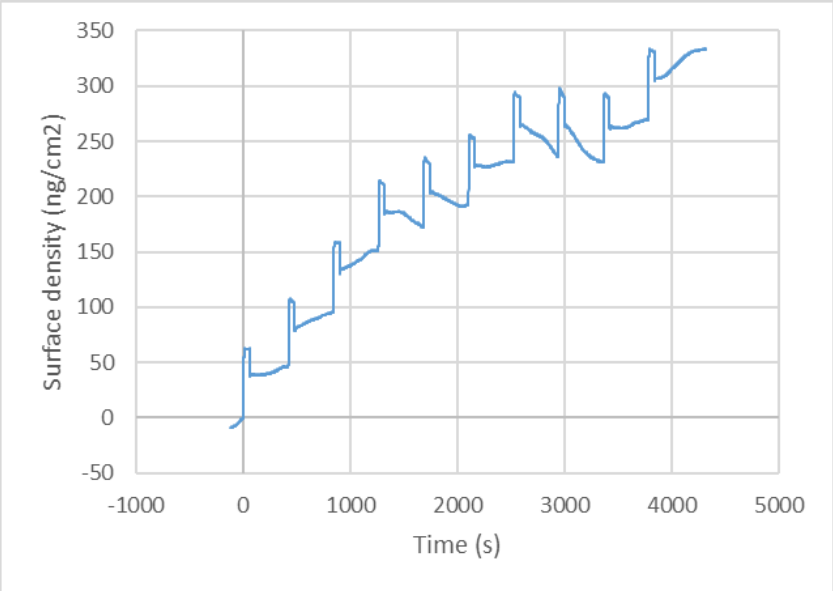

Figure 30 QCM result of NcAP|water at 255˚C (15 second dose of NcAP). (6/28/2022, Run 4)

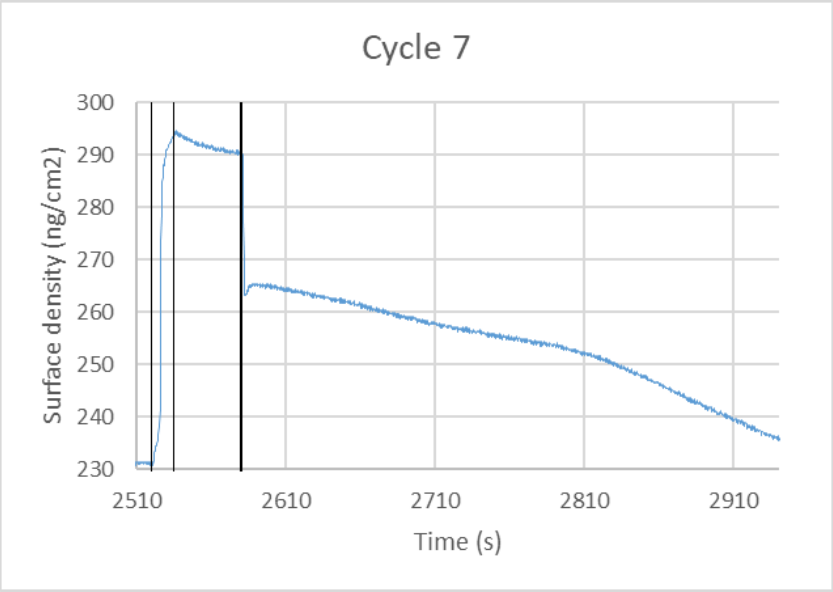

Figure 31 Single ALD cycle of NcAP|water at 255˚C (cycle 7, 15 second dose of NcAP).

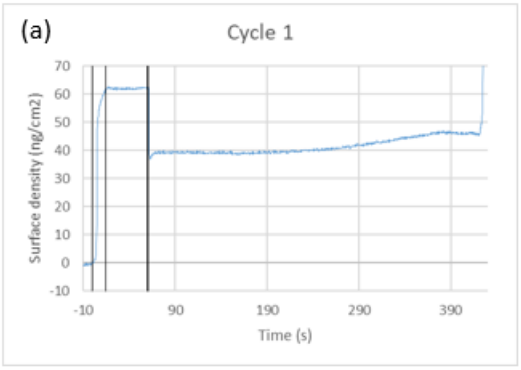

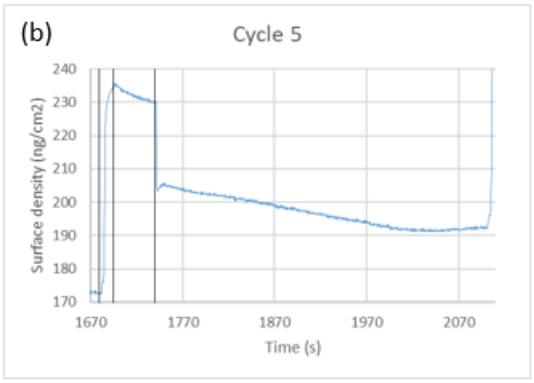

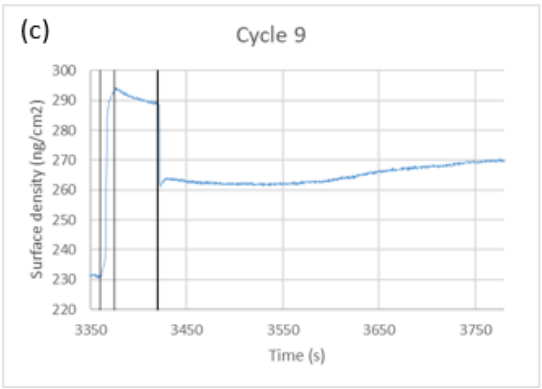

Figure 32 Single ALD cycles of NcAP|water at 255˚C (15 second dose of NcAP), (a) cycle one, (b) cycle five, (c) cycle nine.

Figure 33 shows the QCM result of the deposition process which contains 20 second dose of NcAP. The surface density linearly increased in the first six cycles while there was some drift after cycle seven. After ten cycles of deposition, the surface density increased by 340 ng.cm^{-2}. By zooming in on cycle one, five and nine, it was observed that surface density changed similarly in each single cycle. The surface density increased by 65 ng.cm^{-2} when NcAP was introduced, and decreased by 30 ng.cm^{-2} in the step of water pulse, as shown from figure 34a to c.

The QCM results from both deposition processes are similar, showing that deposition rate does not increase as the dose time of NcAP increases. Self-limiting was observed on the surface so that the deposition process is proved to be ALD.

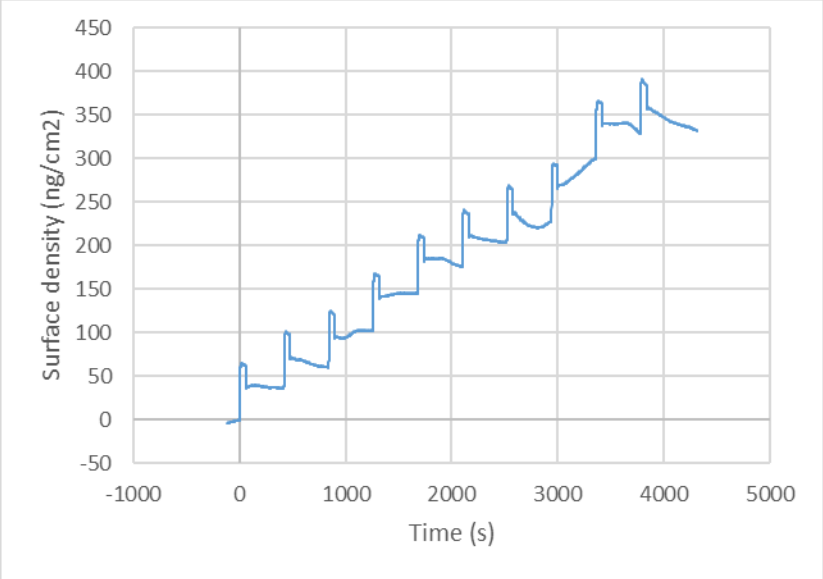

Figure 33 QCM result of NcAP|water at 255˚C (20 second dose of NcAP). (6/28/2022, Run 5)

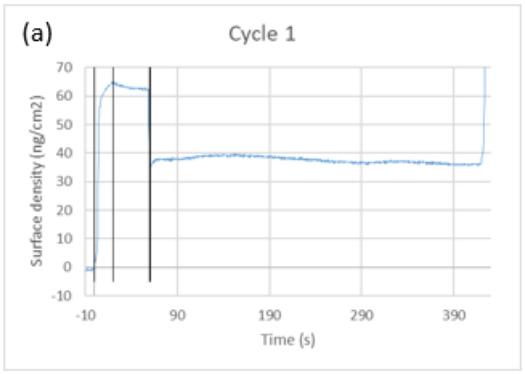

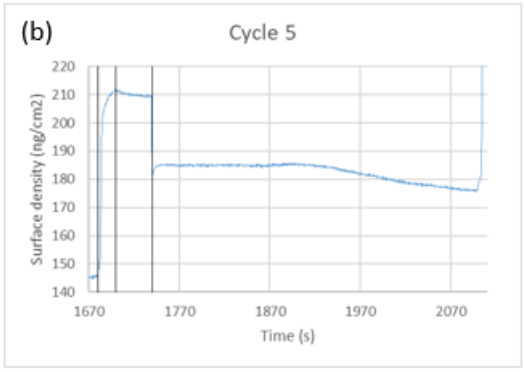

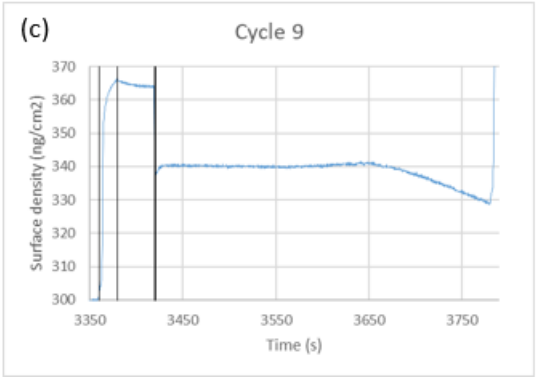

Figure 34 Single ALD cycles of NcAP|water at 255˚C (20 second dose of NcAP), (a) cycle one, (b) cycle five, (c) cycle nine.

4.6 NcAP|water ALD at 285˚C

The chamber temperature was raised to 285˚C to study the temperature window of NcAP. Two deposition processes were conducted, one with 15 second dose of NcAP, followed by 45 second of purge, followed by 0.5 second dose of water, followed by 359.5 second of purge; the other one with 20 second dose of NcAP, followed by 40 second of purge, followed by 0.5 second dose of water, followed by 359.5 second of purge. A gold-coated crystal which is optimized at 285˚C was loaded and saturated with hydroxyl group on the surface before deposition started. The chamber pressure, carrier gas, QCM back side purge, bubbler temperatures, dead zone purge and temperatures of delivery lines were at the same condition used at 150˚C.

Figure 35 shows the QCM result of the deposition process which contains 15 second dose of NcAP. The surface density linearly increased by 264 $ng.cm^{-2}$ after ten cycles of deposition, indicating that GPC at 285˚C is nearly 0.66 $Å.cycle^{-1}$. However, surface density in cycle two, eight and nine was decreased because of drift. Therefore, the GPC calculated by QCM is smaller than the actual value. By zooming in on cycle one, five, and nine, it is apparent that surface density changed similarly in each ALD cycles. The surface density roughly increased by 65 $ng.cm^{-2}$ in the step of NcAP pulse and decreased by 30 $ng.cm^{-2}$ when water was introduced, as shown from Figure 36a to 36c.

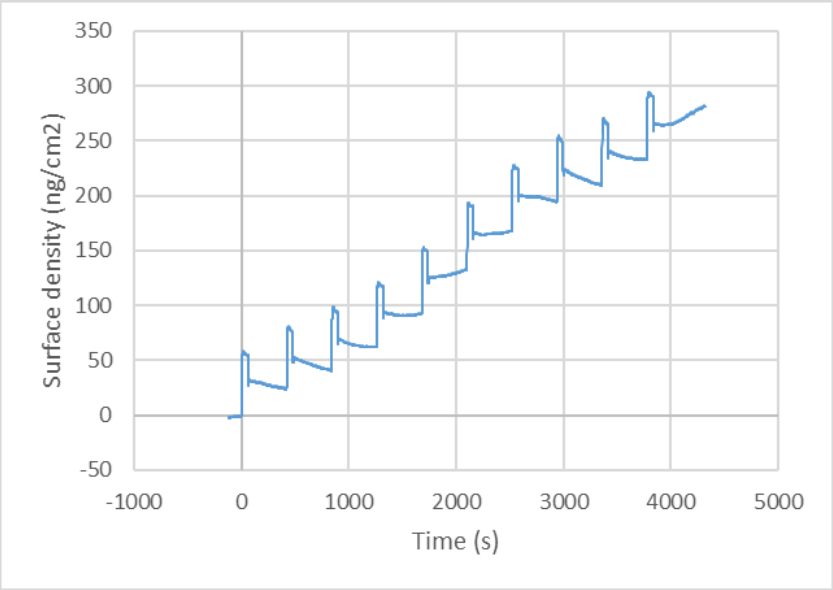

Figure 35 QCM result of NcAP|water at 285˚C (15 second dose of NcAP). (6/27/2022, Run 7)

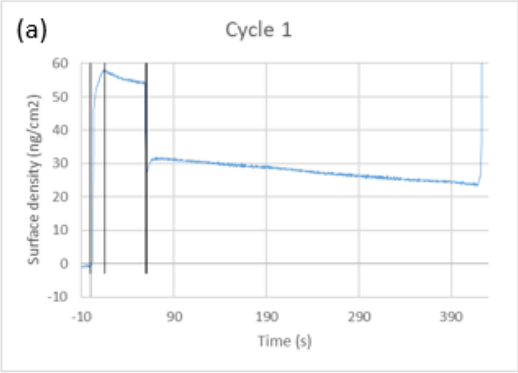

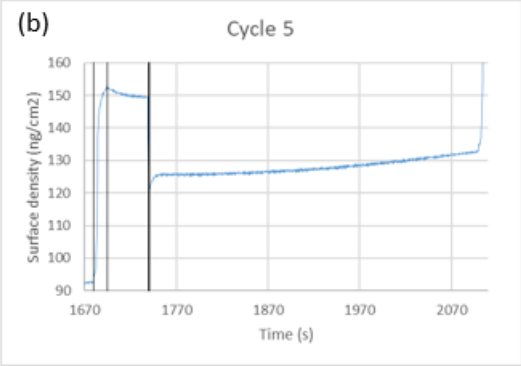

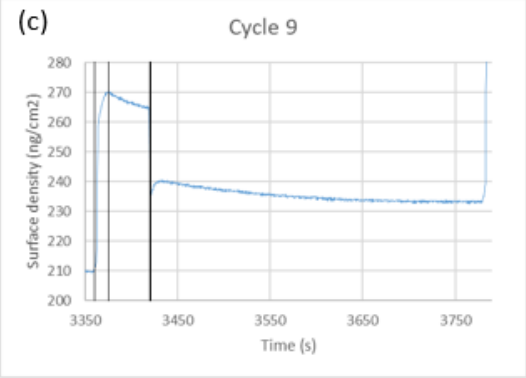

Figure 36 Single ALD cycles of NcAP|water at 285˚C (15 second dose of NcAP), (a) cycle one, (b) cycle five, (c) cycle nine.

Figure 37 shows the QCM result of the deposition process which contains 20 second dose of NcAP. After ten cycles of deposition, the surface density linearly increased by 300 ng.cm^{-2}, indicating that GPC is nearly 0.76 Å.cycle^{-1}. Although the GPC is slightly larger than the result of the 15 second NcAP dose deposition process, there is less drift here. By zooming in on cycle one, five and nine, as shown from Figure 38a to c, surface density was observed to increase by 65 ng.cm^{-2} during NcAP pulses and decrease by 30 ng.cm^{-2} during water pulses. This trend is similar to the result of the 15 second NcAP dose deposition process. The deposition rate does not increase as increasing dose time of NcAP. Hence, the surface was fully saturated by NcAP, and the process was proved to be ALD.

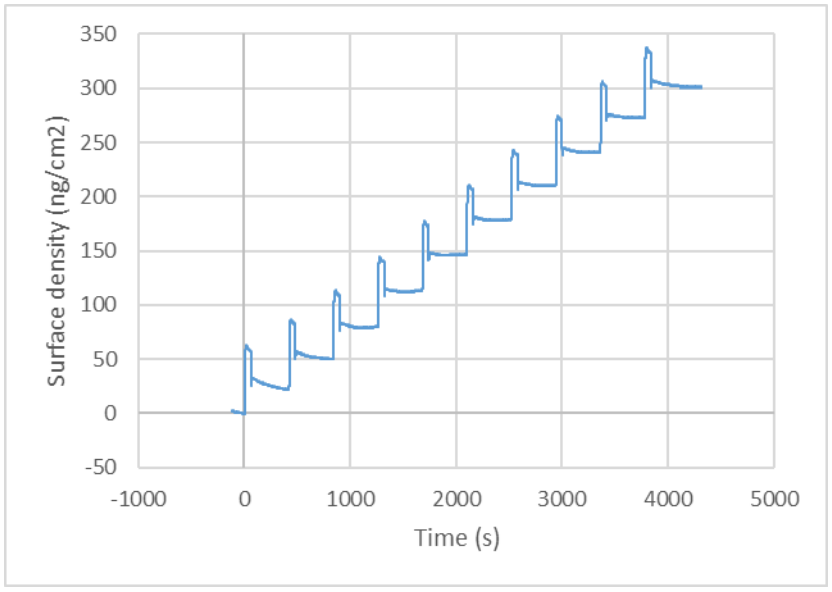

Figure 37 QCM result of NcAP|water at 285˚C (20 second dose of NcAP). (6/27/2022, Run 9)

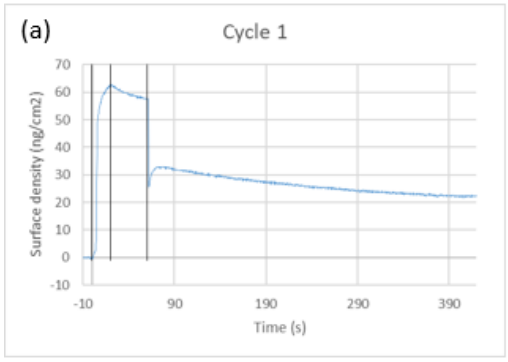

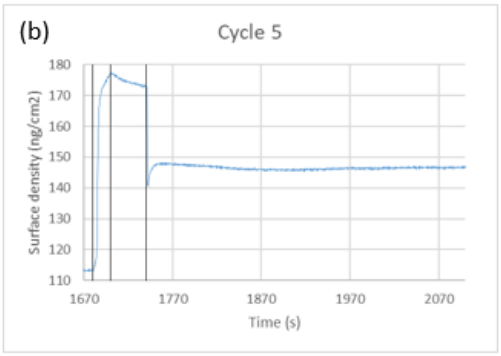

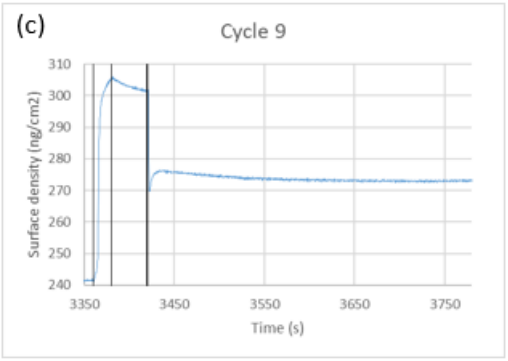

Figure 38 Single ALD cycles of NcAP|water at 285˚C (20 second dose of NcAP), (a) cycle one, (b) cycle five, (c) cycle nine.

5. NcAP Competive Adsorption Study

5.1 Isopropyl alcohol pulses

To obtain area selectivity, co-adsorbate was applied to compete with NcAP for binding sites on the substrate surface. One of the requirements for co-adsorbate is the ability to reversibly adsorb and desorb from the substrate surface. According to the DFT (Density-functional Theory) calculations made by Dr. DiStasio, isopropyl alcohol has tremendous potential for serving as co-adsorbate.

Before applying isopropyl alcohol to AS-ALD, it is vitally important to demonstrate its ability of reversible adsorption. Hence, four cycles of isopropyl alcohol pulses were done at 120˚C. Each cycle consists of 20 second dose of isopropyl alcohol, followed by 70 second of purge. A copper-coated crystal which is optimized at 120˚C was loaded and annealed at 180˚C overnight. During the deposition process, the chamber pressure and temperature were set to 1 Torr and 120˚C, respectively. The isopropyl alcohol bubbler was placed in an ice bath. QCM back side purge was set to 50sccm of argon, and each of the dead zones was purged by 10sccm of gas from cylinder four (97% of argon and 3% of hydrogen). Carrier gas was set to 5sccm flow over the isopropyl alcohol bubbler.

As shown in Figure 39, reversible adsorption and desorption were observed on the copper surface. By zooming in on cycle one and three, as shown in Figure 40a and b, it was apparent that the surface density immediately increased by 16 $ng.cm^{-2}$ and saturated when isopropyl alcohol was introduced. After isopropyl alcohol was turned

off, the surface density instantly dropped back to 0 ng.cm^{-2}. The result shows reversible adsorption and desorption of isopropyl alcohol on copper surface, indicating that isopropyl alcohol can be potentially used as co-adsorbate in AS-ALD.

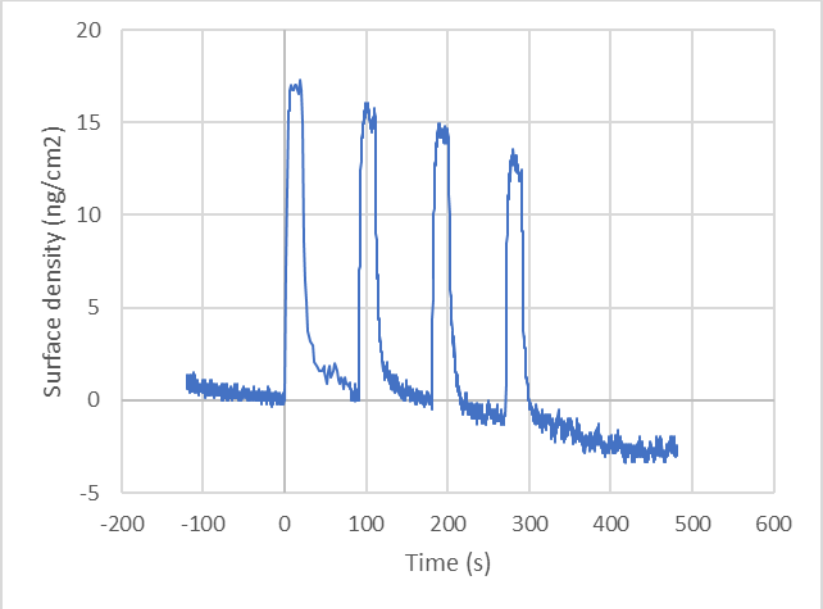

Figure 39 QCM results of isopropyl alcohol pulses at 120˚C. (7/28/2022, Run 2)

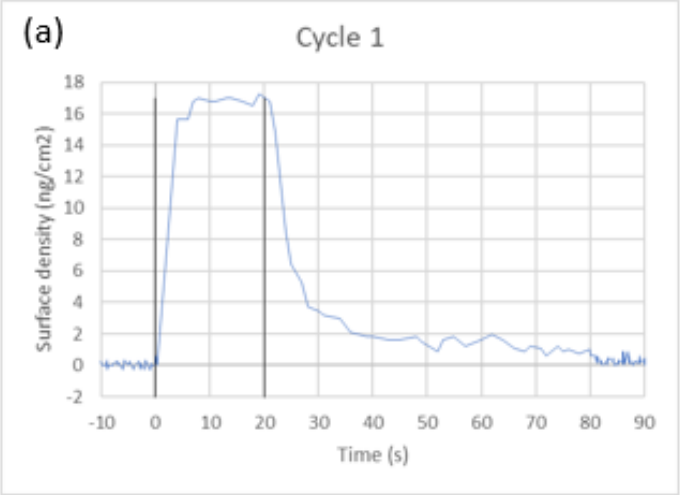

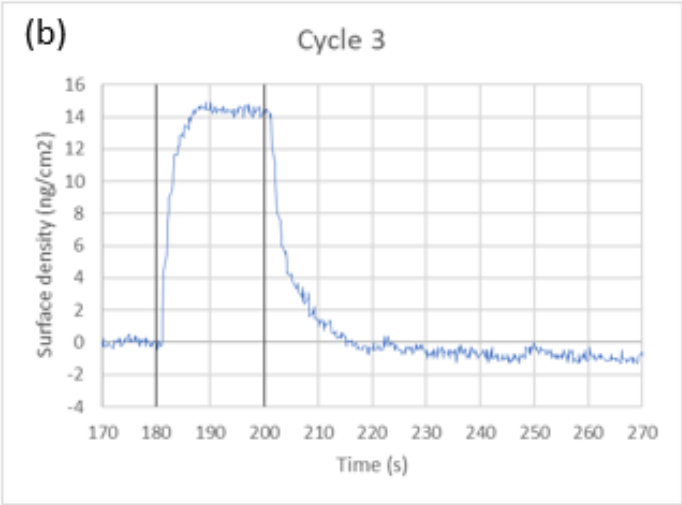

Figure 40 Single cycles of isopropyl alcohol pulses at 120˚C, (a) cycle one, (b) cycle three.

5.2 NcAP|water AS-ALD with isopropyl alcohol

In the AS-ALD process, NcAP, water and isopropyl alcohol were used as precursor, co-reactant, and co-adsorbate, respectively. The process can be expressed as:

Isopropyl alcohol | NcAP/Isopropyl alcohol | Isopropyl alcohol | Purge | water | Purge

In the first half reaction, isopropyl alcohol was firstly introduced to saturate the substrate surface so that all the available binding sites were occupied. In the second step of the process, NcAP and isopropyl alcohol were dosed simultaneously for competitive adsorption. In other words, isopropyl alcohol competed with NcAP for the binding sites on the substrate surface. Afterwards, NcAP was turned off while isopropyl alcohol dose was continued to prevent redeposition of NcAP.

The AS-ALD process was conducted at 120˚C, including 20 cycles of deposition. Each ALD cycle is composed of 15 second dose of isopropyl alcohol, followed by 15 second co-exposure of isopropyl alcohol and NcAP, followed by 15 second dose of isopropyl alcohol, followed by 45 second of purge, followed by 0.5 second dose of water, followed by 359.5 second of purge. Before starting the process, a copper-coated crystal which is optimized at 120˚C was loaded and annealed at 180˚C overnight. The carrier gas was set to 50sccm flow through the NcAP bubbler, 10sccm flow over the water bubbler, and 30sccm flow through the isopropyl alcohol bubbler. The NcAP bubbler was placed in a heat bath and heated to 90˚C, and the water bubbler and the isopropyl alcohol bubbler were placed in an ice bath. The chamber pressure, QCM back side purge, and dead zone purge were at the same condition used at pristine NcAP ALD process.

Figure 41 shows the QCM result after 20 cycles of AS-ALD. The surface density linearly increased by 356 ng.cm^{-2}, indicating that GPC was nearly at 0.45 Å.cycle^{-1}. By zooming in on single ALD cycles, it was observed that the selectivity decreases in the later cycles, as shown from Figure 42a to 42c. When isopropyl alcohol was applied, the surface density rapidly increased by 30 ng.cm^{-2} and plateaued in cycle one and nine, while it increased by 40 ng.cm^{-2} in cycle nineteen. During the co-exposure of isopropyl alcohol and NcAP, the surface density increased by 35 ng.cm^{-2} in cycle one and nine. Nevertheless, the surface density increased by 40 in cycle nineteen. When water was introduced, the surface density decreased immediately, which was similar to ligand exchange observed in pristine NcAP ALD processes. The net increase of surface density is 15 ng.cm^{-2} in cycle one and nine, while it raised to 24 ng.cm^{-2} in cycle nineteen.

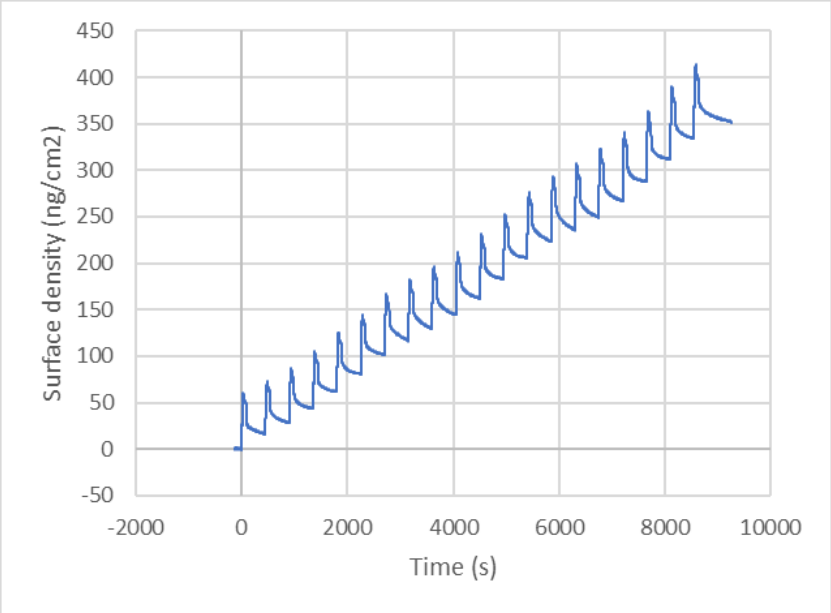

Figure 41 QCM result of NcAP|water|Isopropyl alcohol at 120˚C. (7/7/2022, Run 2)

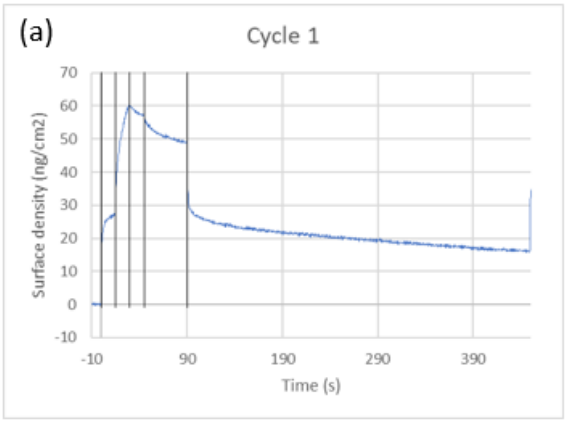

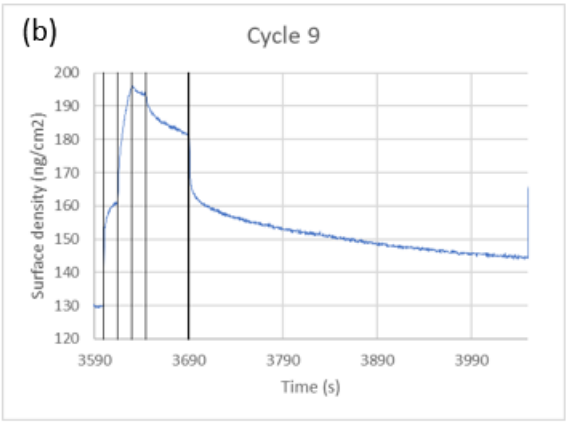

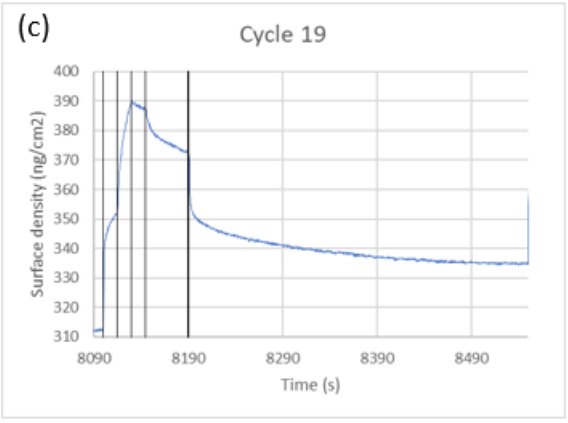

Figure 42 Single ALD cycles of NcAP|water|isopropyl alcohol at 120˚C, (a) cycle one, (b) cycle nine, (c) cycle nineteen.

6. Pristine ZyALD|water ALD Study

6.1 ZyALD pressure study

Tris(dimethylamino)cyclopentadienyl Zirconium (ZyALD) is a zirconium precursor, which has been applied in various fields. For instance, James *et al*. deposited zirconium oxide using ZyALD for fuel cell applications [27]. Park *et al*. used ZyALD and yttrium to deposit films for DRAM capacitors [28].

Before exploring temperature window for ZyALD, it is crucial to demonstrate that it can be delivered by carrier gas in a vacuum chamber. Hence, pressure test of ZyALD was conducted at 120˚C. The ZyALD bubbler was placed in a heat bath and heated to 70˚C. The delivery line of ZyALD was heated to 80˚C to prevent chemical condensation on the inner wall. Carrier gas was set to 50sccm flow through the ZyALD bubbler. The throttle valve opening was fixed at 36.8%, so that the chamber pressure was maintained at 1 Torr before ZyALD was introduced. As Figure 43 shows, 90 seconds after the chamber pressure was recorded, one ZyALD pulse was conducted. When ZyALD was dosed, the chamber pressure raised from 1 Torr to 1.3 Torr, indicating that vapor pressure of ZyALD is 0.3 Torr when ZyALD is at 70˚C. The result shows that the vapor pressure of ZyALD is high enough so that it can be delivered in gas phase and applied to a vacuum system.

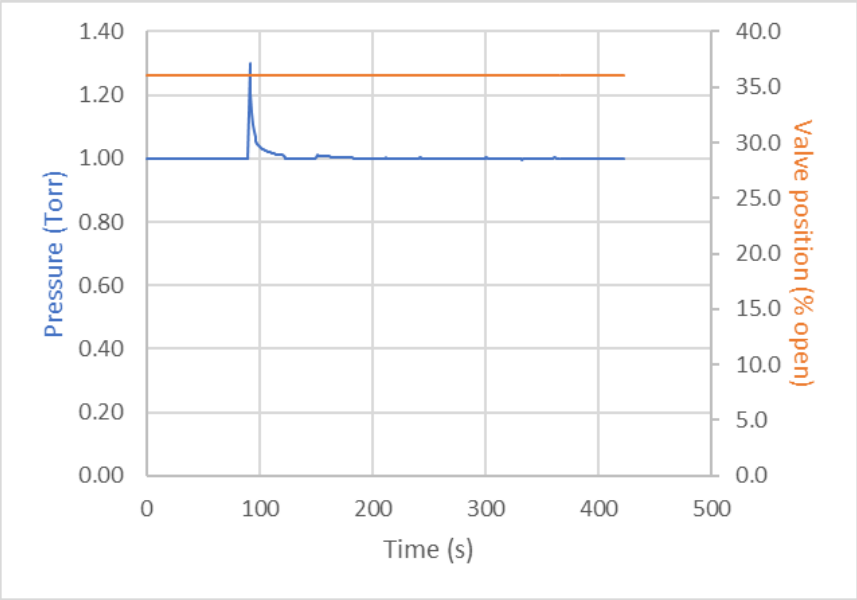

Figure 43 Pressure change during ZyALD pressure test. (8/11/2022, Run 2)

6.2 ZyALD|water ALD at 120˚C

To study temperature window of ZyALD, pristine ALD experiments were conducted at 120˚C and 285˚C. At 120˚C, a gold-coated crystal which is optimized at 120˚C was loaded. Before starting ALD, the crystal surface was coated with ZrO_2 and saturated with hydroxyl group. Each ALD cycle is composed of 20 second dose of ZyALD, followed by 70 second of purge, followed by 0.5 second of water pulse, followed by 359.5 second of purge. The ZyALD bubbler was placed in a heat bath and heated to 90˚C, and the water bubbler was placed in an ice bath. During the deposition process, the chamber pressure was maintained at 1 Torr. The delivery line of ZyALD and water were heated to 90˚C and 80˚C, respectively. QCM back side purge was set to 50sccm of argon and each of the dead zones was purged with 10sccm of gas from cylinder four (97% of argon and 3% of hydrogen). Carrier gas was set to 50sccm flow through the ZyALD bubbler and 10sccm flow over the water bubbler.

Figure 44 shows the QCM result after 10 cycles of ALD at 120˚C. The surface density was linearly increased by 250 $ng.cm^{-2}$, indicating that the growth rate was constantly at 25 $ng.cm^{-2}.cycle^{-1}$. By zooming in on cycle one, five, and nine, as shown from Figure 45a to c, it was observed that the surface density increased by 25 $ng.cm^{-2}$ during the dose of ZyALD. In the step of water pulse, the surface density rapidly increased by 7 $ng.cm^{-2}$ and dropped back to the original value. In contrast to NcAP, the surface density remained the same after water pulse.

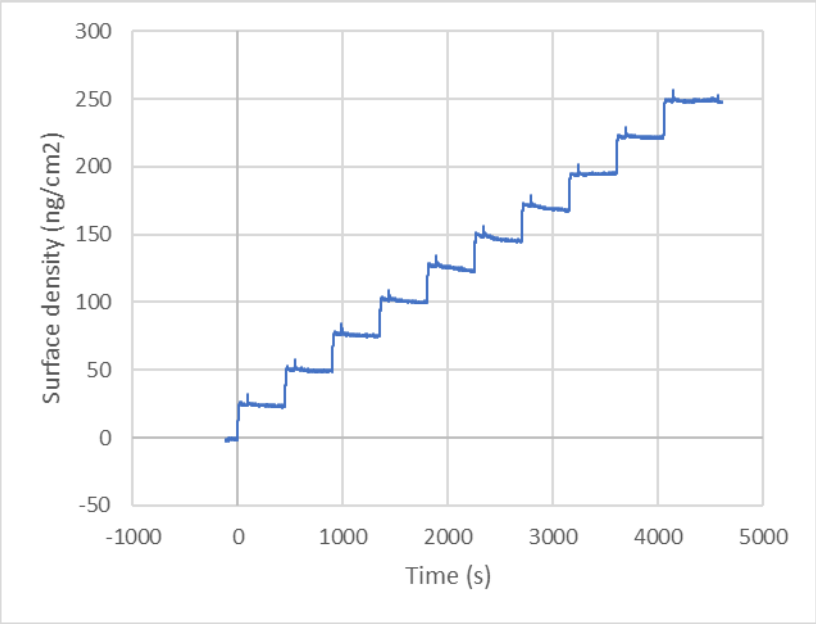

Figure 44 QCM result of ZyALD|water at 120˚C (20 second dose of ZyALD).

(8/19/2022, Run 6)

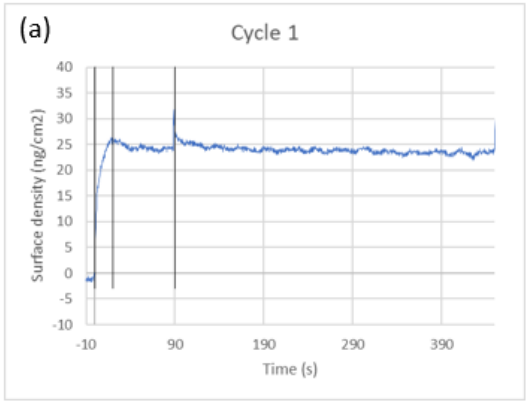

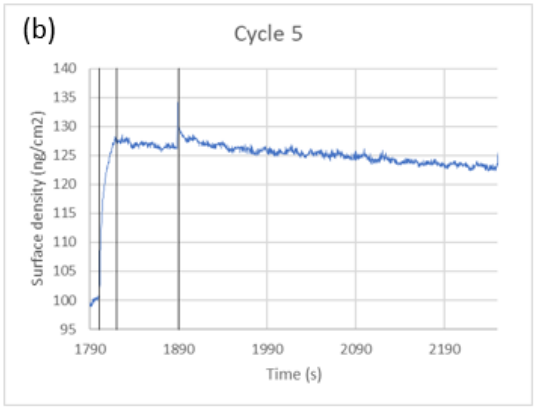

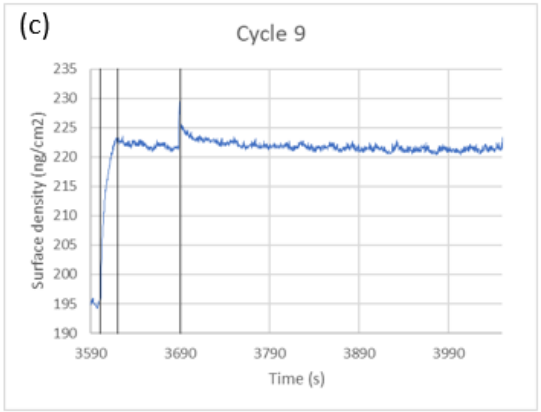

Figure 45 Single ALD cycles of ZyALD|water at 120˚C (20 second dose of ZyALD), (a) cycle one, (b) cycle five, (c) cycle nine.

To ensure the surface was saturated by ZyALD, another pristine ALD process was conducted. Each ALD cycle consists of 40 second dose of ZyALD, followed by 50 second of purge, followed by 0.5 second of water pulse, followed by 359.5 second of purge. As shown in Figure 46, after ten cycles of ALD, the surface density linearly raised by 253 ng.cm^{-2}, which did not significantly increase as the precursor dose time doubled. By zooming in on cycle one, five, and nine, as shown from figure 47a to c, it was observed that the ZyALD growth rate does not increase when ZyALD dose time is doubled. The consistency indicates that self-limiting occurred on the surface and the deposition process was demonstrated to be ALD.

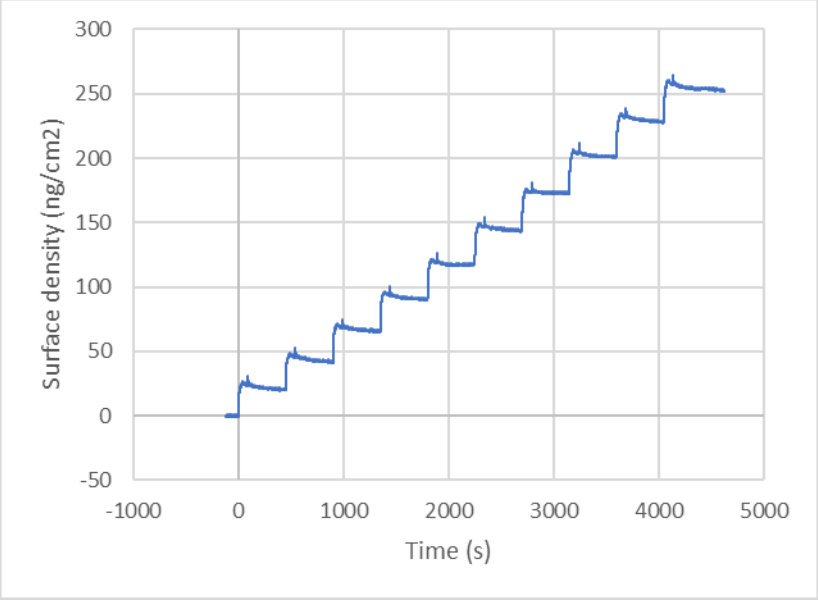

Figure 46 QCM result of ZyALD|water at 120˚C (40 second dose of ZyALD). (8/19/2022, Run 5)

Figure 47 Single ALD cycles of ZyALD|water at 120˚C (40 second dose of ZyALD), (a) cycle one, (b) cycle five, (c) cycle nine.

6.3 ZyALD|water ALD at 285˚C

At 285˚C, a gold-coated crystal which is optimized at 285˚C was loaded. Before starting ALD, the crystal surface was coated with ZrO_2 and saturated with hydroxyl group. Each ALD cycle consists of 20 second dose of ZyALD, followed by 40 second of purge, followed by 0.5 second of water pulse, followed by 359.5 second of purge. The chamber pressure, carrier gas, QCM back side purge, bubbler temperatures, dead zone purge, and temperatures of delivery lines were at the same condition used at 120˚C.

Figure 48 shows the QCM result after 10 cycles of ALD at 285˚C. The surface density linearly increased by 428 $ng.cm^{-2}$, indicating that the growth rate was constantly at 42.8 $ng.cm^{-2}.cycle^{-1}$. By zooming in on cycle one, five, and nine, as shown from Figure 49a to c, it was observed that the surface density increased by 63 $ng.cm^{-2}$ during the dose of ZyALD. The surface density kept decreasing in the purge after precursor dose and dropped by 5 $ng.cm^{-2}$ when water was introduced.

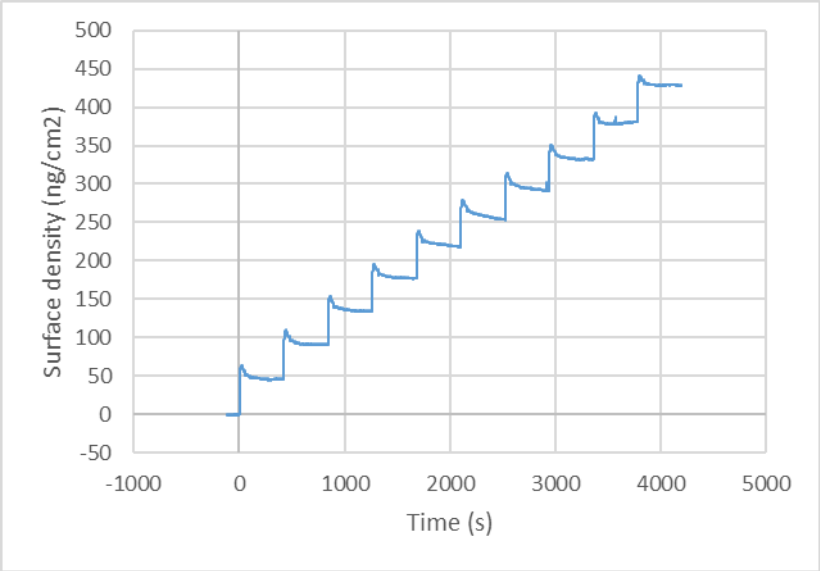

Figure 48 QCM result of ZyALD|water at 285˚C (20 second dose of ZyALD). (9/17/2022, Run 5)

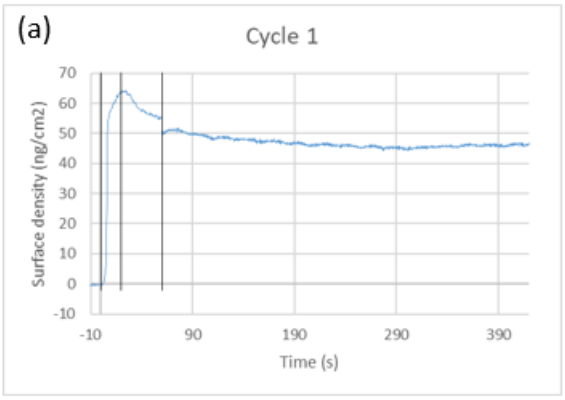

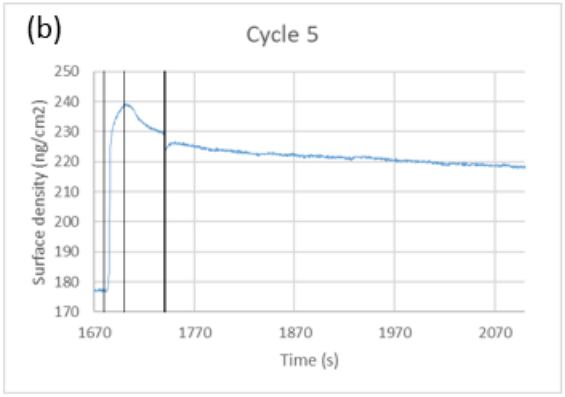

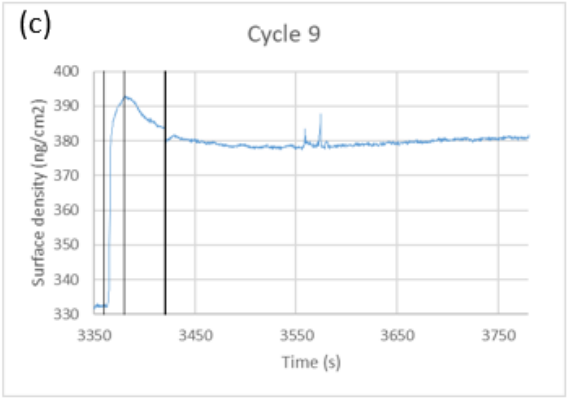

Figure 49 Single ALD cycles of ZyALD|water at 285˚C (20 second dose of ZyALD), (a) cycle one, (b) cycle five, (c) cycle nine.

Another pristine ALD process with extended dose time of ZyALD was conducted to ensure self-limiting was observed. Each ALD cycle is composed of 40 second dose of ZyALD, followed by 50 second of purge, followed by 0.5 second of water pulse, followed by 359.5 second of purge. As Figure 50 shows, the surface density increased by 488 ng.cm^{-2}, which is slightly higher than the value obtained from the 20 second ZyALD dose deposition process. However, changes of surface density in precursor pulse and co-reactant pulse are consistent with the result of 20 second ZyALD dose deposition process, as shown from Figure 51a to c. Hence, the difference between the two deposition processes is resulted from drift. Surface density did not significantly increase as the doubled precursor dose time, showing that the surface was saturated, and the process was proved to be ALD.

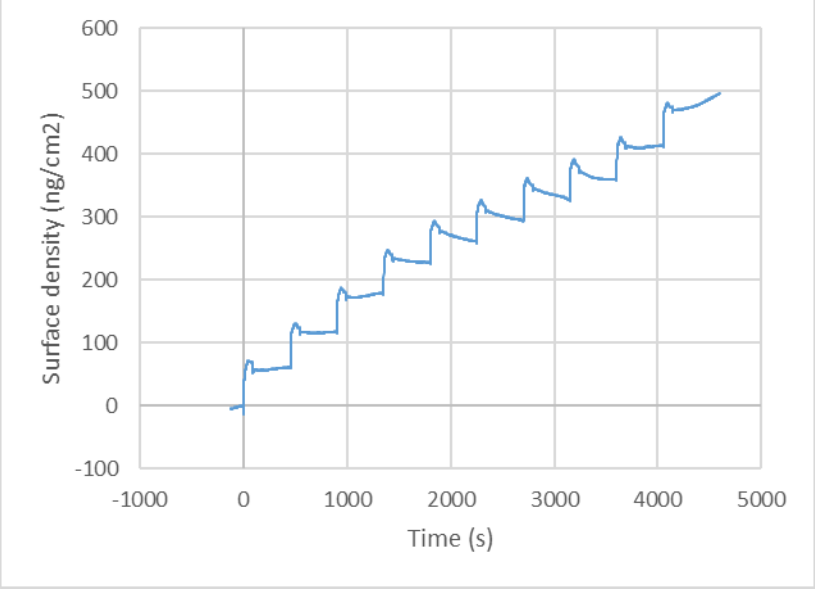

Figure 50 QCM result of ZyALD|water at 285˚C (40 second dose of ZyALD). (8/16/2022, Run 2)

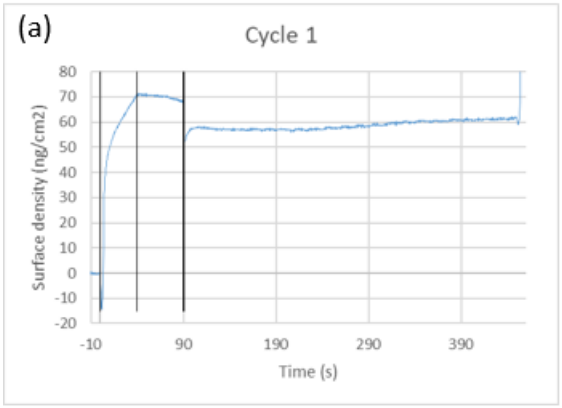

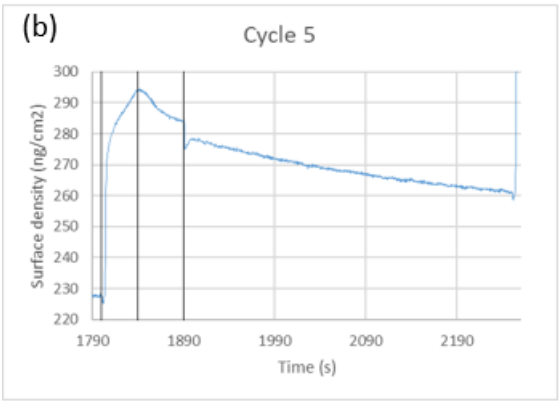

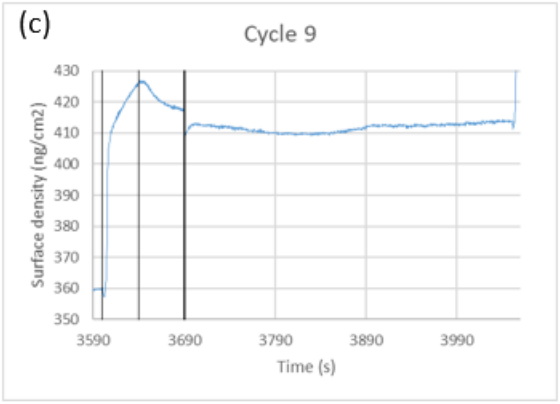

Figure 51 Single ALD cycles of ZyALD|water at 285˚C (40 second dose of ZyALD), (a) cycle one, (b) cycle five, (c) cycle nine.

7. Blocking molecule Study

7.1 Silane blocking molecule pressure study

In AS-ALD, silane has been widely used for passivating surface and blocking ALD growth on it. For instance, Xu *et al*. applied aminosilane to inhibit deposition of Al_2O_3 on SiN_x [29]. Liu *et al*. used octadecyltrimethoxysilane to block ALD growth on SiO_2, and selectively deposited Al_2O_3 and ZnO on copper [30].

Trimethoxypropylsilane was applied to block ZrO_2 ALD growth on Al_2O_3. Before AS-ALD was conducted, vapor pressure of the silane was studied at 285˚C to ensure it can be delivered in vapor phase. The silane bubbler was at room temperature, and delivery line was set to 80˚C. Carrier gas was set to 10sccm flow through the bubbler. The throttle valve opening was fixed at 32.95% so that the chamber pressure was maintained at 1 Torr before dosing silane. As Figure 52 shows, 200 seconds after the pressure was recorded, five trimethoxypropylsilane pulses were conducted. Each of the pulse is composed of 20 second dose of silane, followed by 40 second of purge. When trimethoxypropylsilane was introduced, the chamber pressure raised from 1 Torr to 1.34 Torr, showing that vapor pressure of the silane blocking molecule is 0.34 Torr. The result shows that trimethoxypropylsilane can be delivered in vapor phase, and can potentially be used in AS-ALD.

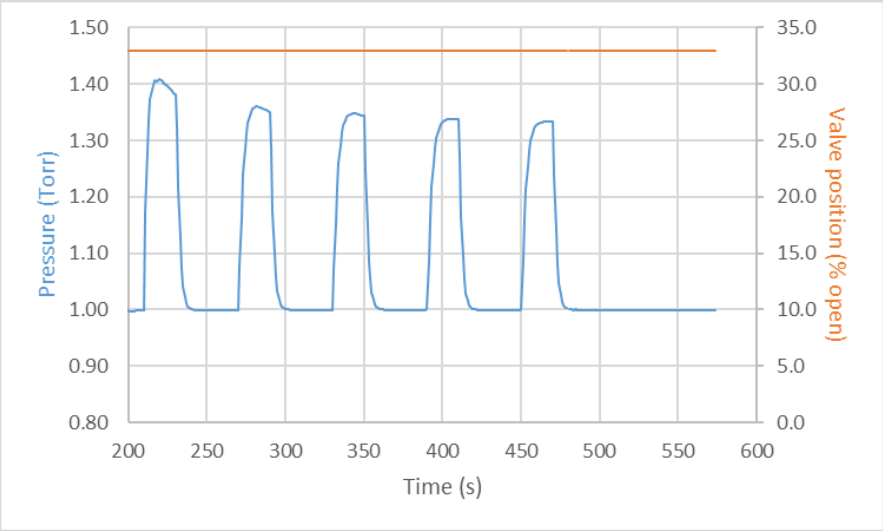

Figure 52 Pressure change during trimethoxypropylsilane pressure test. (10/3/2022, Run 2)

7.2 ZyALD|water AS-ALD with silane blocking molecule

Trimethoxypropylsilane was applied to block the growth of ZyALD on Al_2O_3 surface. The chamber pressure and temperature were maintained at 1Torr and 285˚C, respectively. QCM back side purge was set to 50sccm of argon, and each of the dead zone was purged with 10sccm of gas from cylinder four (97% of argon and 3% of hydrogen). Carrier gas was set to 50sccm flow through the ZyALD bubbler, 10sccm flow over the water bubbler, and 10sccm flow through the trimethoxypropylsilane bubbler. The ZyALD bubbler was placed in heat bath and heated to 90˚C, the water bubbler was placed in ice bath, and the trimethoxypropylsilane bubbler was at room temperature. The delivery line of ZyALD and water were set at 110˚C, and the trimethoxypropylsilane delivery line was set to 90˚C.

A gold-coated crystal which is optimized at 285˚C was loaded. Before introducing trimethoxypropylsilane, 20 cycles of Al_2O_3 ALD were applied to form an alumina layer. As Figure 53 shows, roughly 15.4Å of alumina was deposited on the gold-coated crystal.

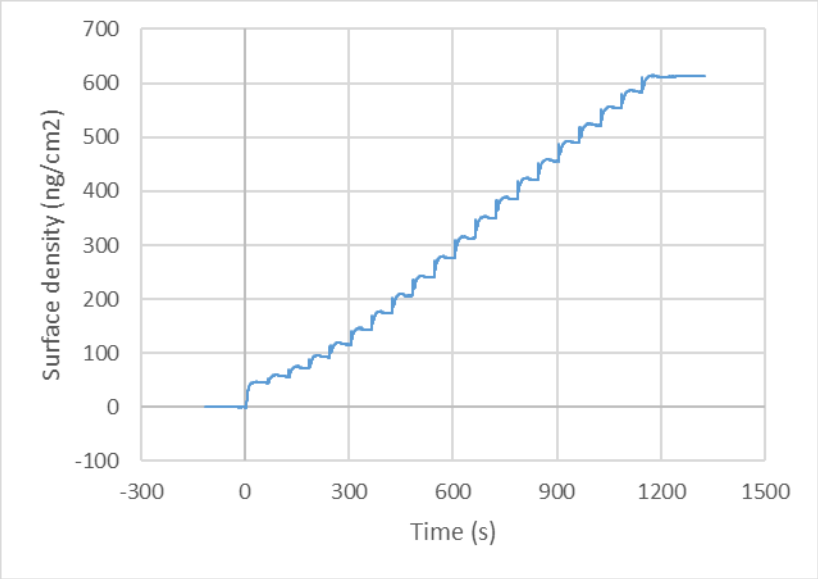

Figure 53 QCM result of depositing Al_2O_3 before starting AS-ALD of ZyALD. (11/10/2022, Run 6)

In contrast to co-adsorbate, silane blocking molecule does not reversibly bind to substrate surface. Hence, silane blocking molecule only needs to be applied before the ALD process, but not during precursor dose. Trimethoxypropylsilane was dosed for 29 minutes to form a passivation layer on the substrate surface.

Ten cycles of ZyALD ALD process were conducted to test the blocking ability of trimethoxypropylsilane. As Figure 54 shows, surface density approximately increased by 140 $ng.cm^{-2}$ (2.4Å) after ten cycles of ALD. By zooming in on cycle one, five and nine, as shown from Figure 55a to c, it was observed that the growth rate of ZyALD was larger in the later cycles. As ALD cycle proceeded, the surface was gradually converted from silane to ZrO_2, which decreased the selectivity. Compared with pristine ALD process, trimethoxypropylsilane suppressed the growth of ZrO_2, as shown in Figure 56.

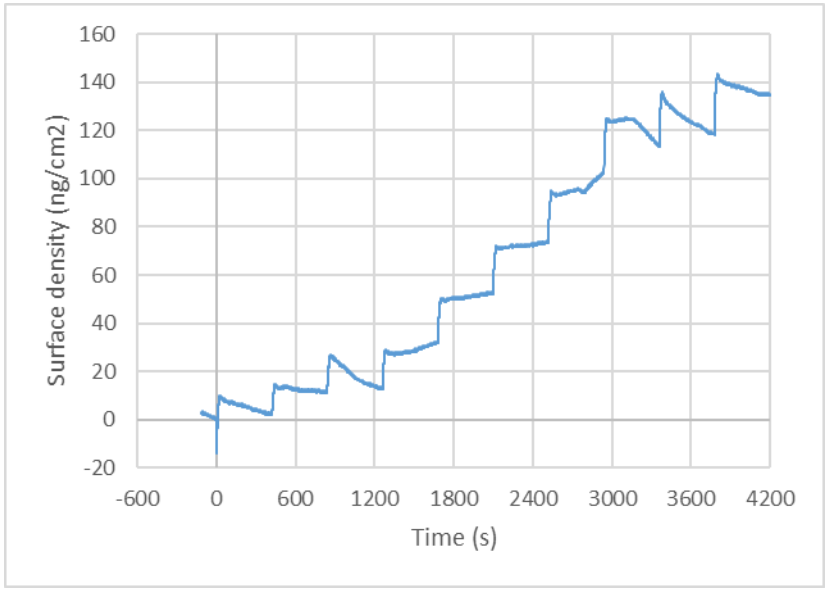

Figure 54 QCM result of ZyALD AS-ALD. (11/10/2022, Run 11)

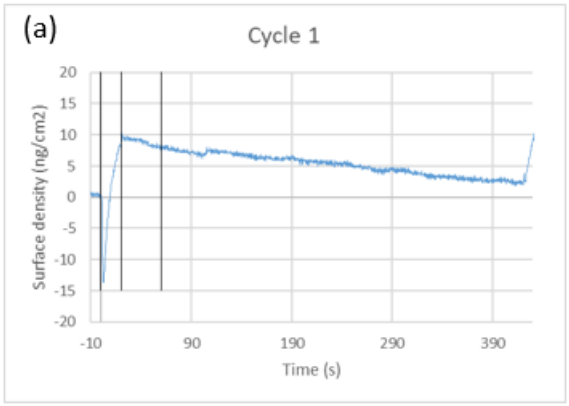

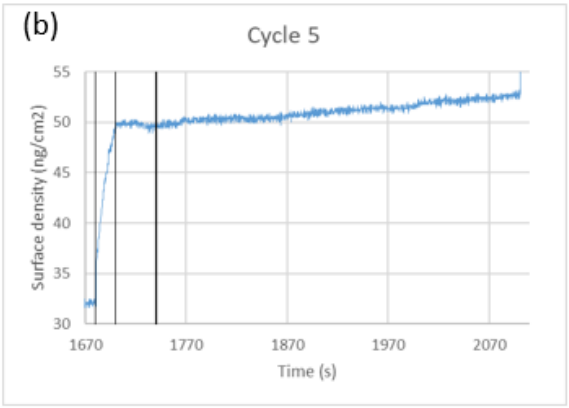

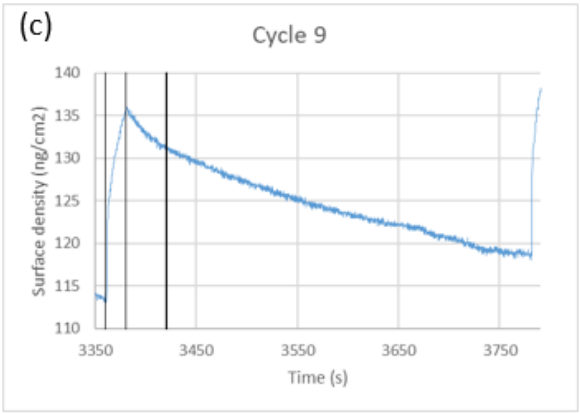

Figure 55 Single ALD cycles of ZyALD AS-ALD, (a) cycle one, (b) cycle five, (c) cycle nine.

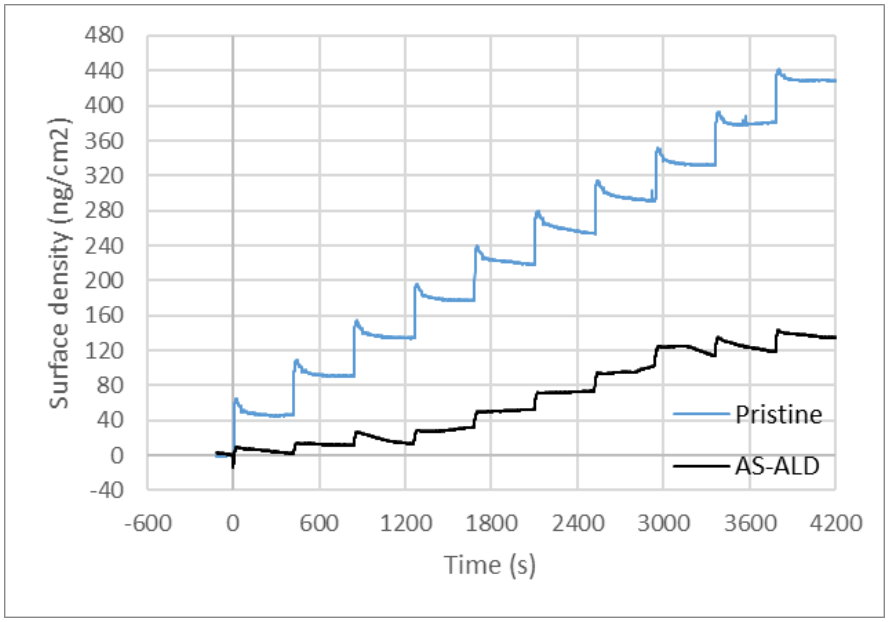

Figure 56 Comparison of pristine ALD and AS-ALD of ZyALD.

8. Conclusions

Several QCM system modifications were made, including installation of purge line to dead zones and replacement of a shorter precursor delivery line. Dead zones could be sources of lingering molecules, resulting in overlap of precursor and co-reactant. A long precursor delivery line could lead to molecular decomposition for unstable precursors. After running a well investigated ALD process of using trimethylaluminum as precursor and water as co-reactant, the published result was reproduced. Self-limiting was observed and GPC is roughly at 1Å.cycle^{-1}.

Nitrogen containing aluminum precursor (NcAP) is a novel precursor which has not been published yet. Temperature window of pristine ALD was explored from 120˚C to 285˚C. Self-limiting was observed because GPC did not raise as increasing dose time of NcAP. In AS-ALD, isopropyl alcohol was used to compete with NcAP for available binding sites on copper, and competitive adsorption decreases GPC from 1 Å.cycle^{-1} to 0.45 Å.cycle^{-1}.

Tris(dimethylamino)cyclopentadienyl Zirconium (ZyALD) was investigated at different temperatures. Recipes of pristine ALD at 120°C and 285°C were developed. In AS-ALD, a silane blocking molecule was used to passivate Al_2O_3 surface and GPC of ZyALD was suppressed.

References

[1] R. R. Schaller, "Moore's law: past, present and future," in *IEEE Spectrum*, vol. 34, no. 6, pp. 52-59, June 1997, doi: 10.1109/6.591665.

[2] G Gay, T Baron, C Agraffeil *et al*. "CMOS compatible strategy based on selective atomic layer deposition of a hard mask for transferring block copolymer lithography patterns" 2010 *Nanotechnology* 21 435301

[3] Adriaan J. M. Mackus, Marc J. M. Merkx, and Wilhelmus M. M. Kessels "From the Bottom-Up: Toward Area-Selective Atomic Layer Deposition with High Selectivity" Chem. Mater. 2019, 31, 1, 2–12

[4] Marc J. M. Merkx, Sander Vlaanderen, Tahsin Faraz *et al.* "Area-Selective Atomic Layer Deposition of TiN Using Aromatic Inhibitor Molecules for Metal/Dielectric Selectivity" Chem. Mater. 2020, 32, 18, 7788–7795

[5] Véronique Cremers, Riikka L. Puurunen, and Jolien Dendooven "Conformality in atomic layer deposition: Current status overview of analysis and modelling" *Applied Physics Reviews* 6, 021302 (2019)

[6] Angel Yanguas-Gil and J. W. Elam "Growth Rate Control in ALD by Surface Functionalization: Alkyl Alcohols on Metal Oxides" 2010 *ECS Trans.* **33** 333

[7] Henrik H. Sønsteby, Angel Yanguas-Gil, and Jeffrey W. Elam "Consistency and reproducibility in atomic layer deposition" *Journal of Vacuum Science & Technology A* 38, 020804 (2020)

[8] Kun Cao, Jiaming Cai, and Rong Chen "Inherently Selective Atomic Layer Deposition and Applications" Chem. Mater. 2020, 32, 6, 2195–2207

[9] Wayne L. Gladfelter, "Selective metalization by chemical vapor deposition" Chem. Mater. 1993, 5, 10, 1372–1388

[10] Dara Bobb-Semple, Katie Lynn Nardi, Nerissa Draeger *et al.* "Area-Selective Atomic Layer Deposition Assisted by Self-Assembled Monolayers: A Comparison of Cu, Co, W, and Ru" Chem. Mater. 2019, 31, 5, 1635–1645

[11] Sameer Patwardhan, Duyen H. Cao, George C. Schatz *et al.* "Atomic Layer Deposition Nucleation on Isolated Self-Assembled Monolayer Functional Groups: A Combined DFT and Experimental Study" ACS Appl. Energy Mater. 2019, 2, 7, 4618–4628

[12] Baolin Zhao, Ziyang Gan, Manuel Johnson *et al.* "2D van der Waals Heterojunction of Organic and Inorganic Monolayers for High Responsivity Phototransistors" Adv. Funct. Mater. 2021, 31, 2105444.

[13] Han-Bo-Ram Lee, Marja N. Mullings, Xirong Jiang *et al.* "Nucleation-Controlled Growth of Nanoparticles by Atomic Layer Deposition" Chem. Mater. 2012, 24, 21, 4051–4059

[14] Rong Chen, Hyoungsub Kim, Paul C. McIntyre *et al.* "Self-assembled monolayer resist for atomic layer deposition of HfO2 and ZrO2 high- κ gate dielectrics" *Appl. Phys. Lett.* 84, 4017–4019 (2004)

[15] Josiah Yarbrough, Alex B. Shearer, and Stacey F. Bent "Next generation nanopatterning using small molecule inhibitors for area-selective atomic layer deposition" *Journal of Vacuum Science & Technology A* 39, 021002 (2021)

[16] Shashank Balasubramanyam, Marc J. M. Merkx, Marcel A. Verheijen *et al.* "Area-Selective Atomic Layer Deposition of Two-Dimensional WS2 Nanolayers" ACS Materials Lett. 2020, 2, 5, 511–518

[17] Wanxing Xu, Paul C. Lemaire, Kashish Sharma *et al.* "Mechanism for growth initiation on aminosilane functionalized SiO2 during area-selective atomic layer deposition of ZrO2" *Journal of Vacuum Science & Technology A* 39, 032402 (2021)

[18] Josiah Yarbrough, Fabian Pieck, Daniel Grigjanis *et al.* "Tuning Molecular Inhibitors and Aluminum Precursors for the Area Selective Atomic Layer Deposition of Al2O3" Chem. Mater. 2022, 34, 10, 4646–4659

[19] Angel Yanguas-Gil, Joseph A. Libera, and Jeffrey W. Elam "Modulation of the Growth Per Cycle in Atomic Layer Deposition Using Reversible Surface Functionalization" Chem. Mater. 2013, 25, 24, 4849–4860

[20] Alfredo Mameli, Marc J. M. Merkx, Bora Karasulu *et al.* "Area-Selective Atomic Layer Deposition of SiO2 Using Acetylacetone as a Chemoselective Inhibitor in an ABC-Type Cycle" ACS Nano 2017, 11, 9, 9303–9311

[21] Wanxing Xu, Mitchel G. N. Haeve, Paul C. Lemaire *et al.* "Functionalization of the SiO2 Surface with Aminosilanes to Enable Area-Selective Atomic Layer Deposition of Al2O3" Langmuir 2022, 38, 2, 652–660

[22] Taewon Suh, Yan Yang, Pengyuan Zhao *et al.* "Competitive Adsorption as a Route to Area-Selective Deposition" ACS Appl. Mater. Interfaces 2020, 12, 8, 9989–9999

[23] Taewon Suh, Yan Yang, Hae Won Sohn *et al.* "Area-selective atomic layer deposition enabled by competitive adsorption" *Journal of Vacuum Science & Technology A* 38, 062411 (2020)

[24] Hossein Salami, Andrew Poissant, and Raymond A. Adomaitis "Anomalously high alumina atomic layer deposition growth per cycle during trimethylaluminum under-dosing conditions" *Journal of Vacuum Science & Technology A* 35, 01B101 (2017)

[25] Marc J. M. Merkx, Athanasios Angelidis, Alfredo Mameli *et al.* "Relation between Reactive Surface Sites and Precursor Choice for Area-Selective Atomic Layer Deposition Using Small Molecule Inhibitors" J. Phys. Chem. C 2022, 126, 10, 4845–4853

[26] Job Soethoudt, Yoann Tomczak, Ben Meynaerts *et al.* "Insight into Selective Surface Reactions of Dimethylaminotrimethylsilane for Area-Selective Deposition of Metal, Nitride, and Oxide" J. Phys. Chem. C 2020, 124, 13, 7163–7173

[27] C. James, R. Xu, G. Jursich *et al.* "Atomic Layer Deposition of Zirconium Oxide for Fuel Cell Applications" The Journal of Undergraduate Research at the University of Illinois at Chicago 5, (2012). doi:10.5210/jur.v5i1.7505.

[28] Bo-Eun Park, Il-Kwon Oh, Chandreswar Mahata *et al.* "Atomic layer deposition of Y-stabilized ZrO2 for advanced DRAM capacitors" *Journal of Alloys and Compounds* Volume 722, 25 October 2017, Pages 307-312

[29] Wanxing Xu, Ryan J. Gasvoda, Paul C. Lemaire *et al.* "Area-selective atomic layer deposition of Al2O3 on SiNx with SiO2 as the nongrowth surface" *Journal of Vacuum Science & Technology A* 40, 012403 (2022)

[30] Tzu-Ling Liu, Maggy Harake, and Stacey F. Ben "Sequential Use of Orthogonal Self-Assembled Monolayers for Area-Selective Atomic Layer Deposition of Dielectric on Metal" *Adv. Mater. Interfaces* 2023, 10, 2202134